Available online at www.sciencedirect.com
SCIENCE DIRECT®
Coordination Chemistry Reviews 249 (2005) 2458–2488
COORDINATION CHEMISTRY REVIEWS
www.elsevier.com/locate/ccr

Review

Supramolecular chemistry and complexation abilities of diphosphonic acids

Ewa Matczak-Jon*, Veneta Videnova-Adrabińska

Department of Chemistry, Wrocław University of Technology, Wybrzeże Wyspiańskego 27, 50-370 Wrocław, Poland

Received 31 December 2004; accepted 9 June 2005
Available online 9 August 2005

Contents

Abstract

The solution and solid state complexation features for two classes of diphosphonic acids: with *gem*-phosphonic–phosphonate groups or with a C–N–C spacer between them are reviewed. In particular, the co-ordination and the supramolecular networks in their complexes are discussed. The structural analysis revealed a large variety of coordination units, dependent upon the topochemical nature of the ligands, the geometrical and charge preferences of the metal ions, and the influence of the counter ions. An amazing superstructural and supramolecular

* Corresponding author. Tel.: +48 71 320 41 34; fax: +48 71 328 43 30.
E-mail addresses: e.jon@ch.pwr.wroc.pl (E. Matczak-Jon), veneta@pwr.wroc.pl (V. Videnova-Adrabińska).

doi:10.1016/j.ccr.2005.06.001

diversity is observed in the extended frameworks. The solution-solid state relationships are elucidated and the role of the hydrogen bonds for the metal complexation in solution is also revealed.

Keywords: Diphosphonic acid; Complexation capabilities; Coordination networks

1. Introduction

Diphosphonic acids, $PO_3H_2–X–PO_3H_2$, constitute a versatile class of bifunctional compounds, in which each phosphonate group can provide one, two or three oxygen atoms to co-ordinate metal ions. In addition, their chemistry can be modulated by variations in the X tether length and/or incorporation of additional functional groups to it. Here, we discuss two important subclasses of this group: with *gem*-phosphonic–phosphonate groups or with C–N–C spacer between them. The compounds of interest are presented in Scheme 1.

Some diphosphonic acids with the P–C–P backbone, commonly named bisphosphonates, have been known since the 19th century. Initially, they were used mainly as antiscaling and anticorrosive agents but also as complexing agents in the textile, fertilizer and oil industries [1]. The attempts in 1960s to find new functional agents resembling the pyrophosphate as a physiological regulator of calcification and bone resorption [2] resulted in the discovery of the bone resorption inhibition properties of bisphosphonates, which, contrary to the pyrophosphates, are not subjected to rapid hydrolysis. The P–C–P structure in bisphosphonates secures stability towards heat and most chemical reagents and a complete resistance to enzymatic hydrolysis. The first bisphosphonates successfully used in the clinic in the 1970s and 1980s were etidronate (**2**) and chlodronate (**3**). Similar to pyrophosphate they have a high affinity for bone mineral and at high doses modulate calcification both in vivo and in vitro. The search for more potent bisphosphonates accomplished the discovery of a number of new compounds with longer side chains than the methyl group of **2**, and with a nitrogen atom as a key struc-

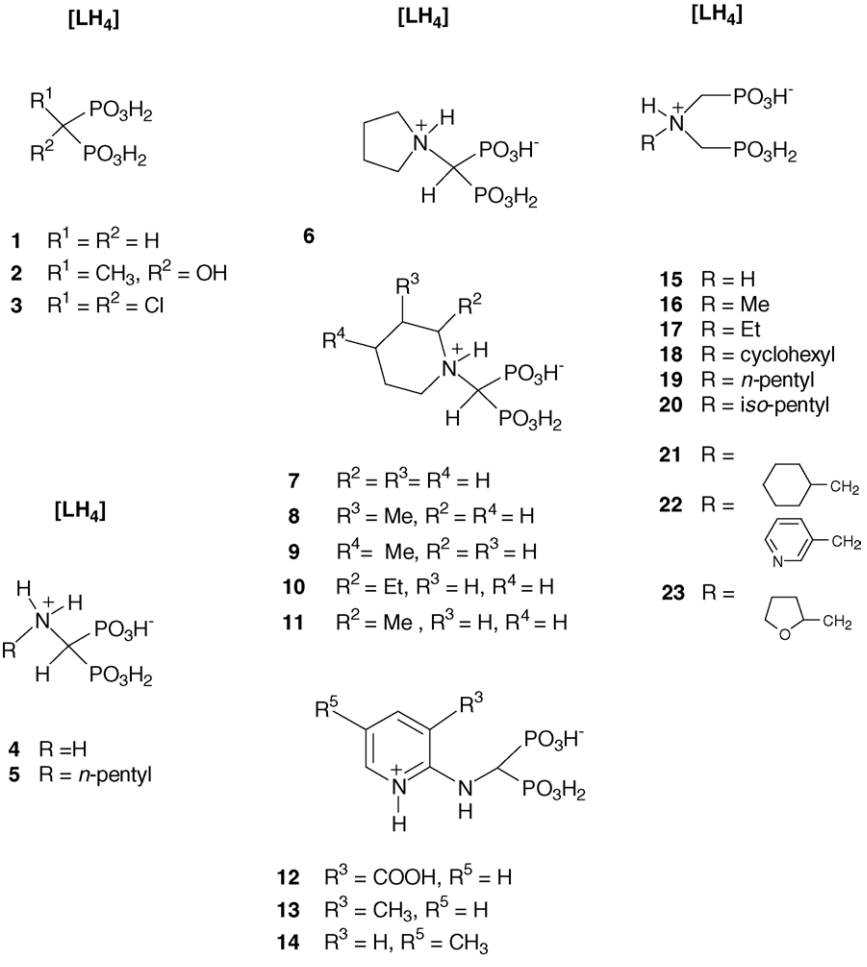

Scheme 1. The compounds under consideration.

tural element for an increase in their potency. In particular, compounds containing a basic primary nitrogen atom were found to be 10–100 times more potent, while those with a nitrogen atom within a heterocyclic ring were up to 10,000 more potent as compared to etidronate [3–8].

Much of the importance of bisphosphonates in their use in bone disorder treatments derives from their strong affinity to metal ions. In particular, the interference with Ca^{2+} and Mg^{2+} is of vital importance for their activity. The *gem*-bisphosphonate groups impart a high affinity for calcium pyrophosphate due to their ability to chelate calcium ions, thus are required for drug targeting to the bone mineral. In addition their presence is indispensable for the molecular mechanism of action of bisphosphonates. It was only recently found that the action of the nitrogen-containing bisphosphonates on the osteoclastic bone resorption is a result of the inhibition of one enzyme in the mevalonate pathway, namely the farnesyl pyrophosphate (FPP) synthase [7–17]. The binding of the substrate or the bisphosphonate inhibitor to the active site of this enzyme takes place with the participation of a cluster consisting of three Mg^{2+} ions, as demonstrated by recent X-ray diffraction studies [18]. The mevalonate pathway is also essential for the synthesis of a variety of sterols and polisoprenoid compounds, which are of vital importance for parasitic protozoa survival in vitro and in vivo [19]. The most potent bisphosphonate inhibitors of parasite growth, including those applied in bone resorption therapy [19–23] and the aminomethane-1,1-diphosphonic acids [24,25], appear also to be potent FPP synthase inhibitors. However, it is still not clearly understood why small structural modifications of the bisphosphonates may lead to extensive alterations in their physicochemical, biological and toxicological characteristics. In this respect a detailed structure-correlated study of the individual properties and the complex-forming driving factors is desired in order to sufficiently understand bisphosphonate physiological activity.

Iminodimethylenediphosphonic acids, despite being considered as structural analogues of the popular herbicide *N*-phosphonomethylglycine (glyphosate) [26], display negligible biological activity [27].

The diphosphonate solid state coordination chemistry was initially focused on a design of hybrid inorganic–organic materials with respect to their eventual application as catalysts, molecular sieves, non-linear optical materials and others [28–33]. Many diphosphonate complexes have been structurally characterized either by a single crystal diffraction technique or from X-ray powder diffraction data. A survey in Cambridge Structural Database (V5.25) [34–36] reveals a large variety of structural units and motifs and the structures range from one-dimensional (1D) chains, two-dimensional (2D) layers to three-dimensional (3D) coordination frameworks. The factors that determine these structures include the length and/or nature of the organic spacer, the extent of protonation of the phosphonate groups, the geometrical preferences and charge of the coordinated metal ion and the influence of the inorganic or organic cations when applicable. In this review, we make an effort to compare and schematize the infinite architecture of these complexes using a modified topological approach for analysis of metal–organic frameworks (MOF). Originally, the principles for delineation of metal–organic frameworks were developed by Robson and co-workers [37] and successfully used for a topological classification of variable interpenetrating nets [38]. The method was very helpful in recognition of a wide classes of polycatenated and polythreaded species [39]. In view of the fascinating abilities of bisphosphonates as ligands and the large number of variable coordination units and structurally diverse linking motifs, a specification of the individual coordination units and the motifs linking them in extended coordination framework is highly desired. In our opinion this approach might be useful for both: the design of new structurally based materials and to understand their structure dependent complex-forming abilities in solution.

2. General properties of diphosphonic acids with formula $PO_3H_2–X–PO_3H_2$

It is common for diphosphonic acids that only two protons are released from the phosphonate PO_3H^- groups upon successive base titration in solution, provided that no additional functional groups are involved. This is due to the fact that the first proton on the phosphonic PO_3H_2 group is very acidic and dissociates out of the measurable range of pH. In addition, the PO_3H^- groups differ in acidities [40–48]. This is particularly significant in methane-1,1-diphosphonic acid and its derivatives [40–45] and is explained by the fairly strong electronic interactions between the two charged close-lying *gem*-diphosphonate groups. Generally, the attachment of a basic nitrogen atom to the molecule increases the acidities of both PO_3H^- groups. This seems to be particularly relevant to compounds, in which the NH^+ proton is very basic [45]. The $pK_{(PO_3H^-)}$ values of compounds bearing a weakly basic protonation site, like *N*-2-pyridyl-derivatives, remain similar to those of the parent methane-1,1-diphosphonic acid except for cases when the electronic effects of the pyridyl substituent are significant [40].

The nitrogen proton in aminomethane-1,1-diphosphonic acids is generally more basic when compared to iminodimethylenediphosphonic acids [40,45,47,48]. This can be attributed to the intramolecular N–H···O (phosphonic–phosphonate) hydrogen bonds, found in most of the crystals studied and retained also in solution [49,50]. The only exception is a group of aminomethane-1,1-diphosphonic derivatives with heteroaromatic amines directly attached to the N-atom as the side chains. For example, the attachment of the pyridyl substituent, which is less basic versus the amino group, results in protonation on the pyridine nitrogen atom [49,51,52].

One of the most significant features of diphosphonic acids is their strong potential to form extensive hydrogen-bonded networks, which is a consequence of the tetrahedral

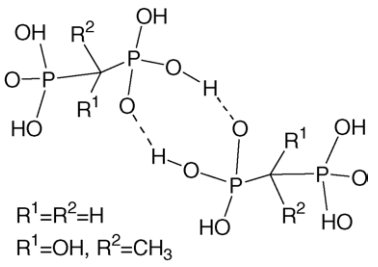

Scheme 2. Basic structural $R_2^2(8)$ ring motif in **1** and **2**.

geometry of the phosphonate and/or phosphonic groups and their hydrogen-bond donor and acceptor capabilities. In contrast to **1**-**3**, in which the phosphonic groups remain fully protonated in solid state [53–55], compounds with a primary or secondary nitrogen atom in the structure always exist as zwitterions with the proton transferred from one of the phosphonic group to the nitrogen atom [48–52,56–62]. The protonated nitrogen involved in inter- and/or intramolecular hydrogen bonds plays an important role for the molecular organization in solid state and solution, as well as for the complex-forming abilities of the compound.

3. Methane-1,1-diphosphonic acid and derivatives

3.1. Solid state molecular organization and hydrogen-bonded networks in methane-1,1-diphosphonic and 1-hydroxyethane-1,1-diphosphonic acids

Compounds **1** and **2** [53–55] are isomorphic and crystallize in the monoclinic system, $P2_1/c$ space group. The molecules are strongly predisposed for mutual recognition via hydrogen-bond interaction between the end positioned phosphonic groups. The three-dimensional hydrogen-bonded network in **1** is executed by four relatively strong hydrogen bonds (O···O from 2.58 to 2.67 Å) formed between the two different phosphonic groups $P(1)O_3H_2$ and $P(2)O_3H_2$ of neighboring molecules. In particular, each phosphonic group donates two different hydrogen bonds towards the P(1), P(2) oxygen sites of neighboring molecules and accepts two others from neighboring molecules. A more detailed structural insight revealed the centrosymmetric ring motif $R_2^2(8)$ (Scheme 2) executed by a head-to-head P(1)O–H···O=P(1) hydrogen-bond interaction to be the basic structural motif in **1**. Two other hydrogen bonds P(2)O–H···O=P(1) and P(1)O–H···O=P(2) are used for the organization of the molecular dimers into thick molecular (1 0 0) layers. A bigger ring motif $R_3^3(16)$ is generated in the interior of the layer from the combination of three different hydrogen bonds. The P(2)O–H···O=P(2) hydrogen bond joins the layers into porous 3D hydrogen-bonded network with a generation of another ring motif $R_4^2(16)$ in the interlayer region (Fig. 1a and b).

The molecular organization in the crystal network of **2** is different due to topochemical differences in the

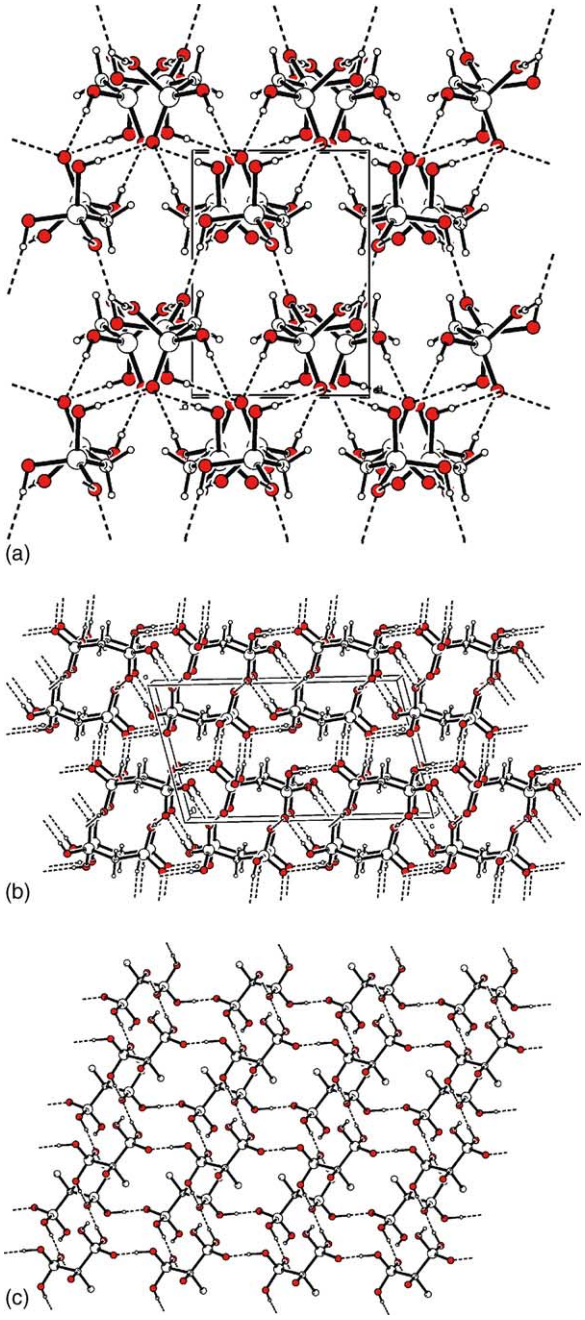

Fig. 1. Two different side views of the molecular monolayers of **1** demonstrating the hydrogen bonds in them (a), between them (b) and the monolayer of **2** (c).

spacer between the two phosphonic groups $P(1)O_3H_2$ and $P(2)O_3H_2$ and the additional hydrogen-bond donor site on the alcoholic group. The hydrogen-bonded dimers $R_2^2(8)$, formed by P(1)O–H···O=P(1), are extended into ribbons via a $R_2^2(12)$ motif. Translation related ribbons are arranged into a 2D network with two more windows $R_4^4(16)$ and $R_4^4(20)$ (Fig. 1c). However, due to the size and geometry of the spacer, the molecular monolayers in **2** undulate and direct phosphonic–phosphonic interactions are prevented. Instead of this, the C–OH hydrogen-bond donor sites,

arranged outward from both sides of the monolayer are used to furnish the 3D network via (C)O–H···O=P(2) interaction. A very large ring motif $R_6^4(22)$ is generated in the interlayer region. Crystal water is incorporated in the interlayer region forming water channels running through the $R_6^4(22)$ rings and additionally bridging the layers.

3.2. Complex-forming abilities in solution

The high potential for effective binding of various metal ions in solution is a key feature of all compounds with *gem*-diphosphonate groups attached to the α-carbon atom. This is attributed to the suitable steric arrangement of phosphonate groups with oxygen sites predisposed for bidentate or bis-bidentate binding mode, as well as to their propensity to form stable protonated complexes, even in solutions of relatively high acidity. The alcoholic OH in **2** is also a potential donor group, but its role for metal complexation in solution is not yet clear.

The speciation of complexes of **1** and **2** with transition and non-transition metal ions has been widely studied through the potentiometric method [41,63–71]. Even alkaline metal ions are detected to form weak complexes with **1** and **2** [71]. Most of the potentiometric models used in calculations consider only mononuclear $[MH_2L]$, $[MHL]^-$ and non-protonated $[ML]^{2-}$ complexes of divalent cations to exist in solution. Generally, the coordination of a second ligand in order to form bis-complexes is considered to be less favored due mostly to high electrostatic repulsions between the negatively charged phosphonate groups around the metal ion. The chelation via oxygen atoms of both phosphonate groups with a resultant six-membered ring formation is a widely accepted coordination mode in both protonated and non-protonated mononuclear complexes of **1** and **2**. The stability constants of the $[ML]^{2-}$ complexes with several divalent cations are presented in Table 1.

In addition, the formation of dimeric $[M_2L]$ species of alkaline earth Mg^{2+} with **1** and Ca^{2+} with **2** were revealed in solution [64,69,70]. Compound **2** was also found to form weak $[M_2L]^{2-}$ complex with Li(I) [71]. and precipitates of metal-to-ligand 2:1 stoichiometry were isolated from the systems with Pb^{2+} and Cd^{2+} [68]. A very recent reinvestigation of the Cu^{2+} system with **2** revealed the prevalence of the oligomeric complex in the intermediate pH range 6–8 along with some minor 1:1 and 1:2 species [41]. The existence of the monomer ⇌ oligomer equilibrium was proven both by spectrophotometry and EPR where a new set of signals arising from the oligomeric species was detected. So, the 3:3 metal-to-ligand complex is assumed to predominate, adopting a bis-bidentate binding mode with an alcoholic group retained in the protonated form (Scheme 3a). Although the existence of alcoholic-OH forms seems to be a common feature for most complexes with divalent metal ions, the deprotonation of OH induced by the metal ion should always be taken into consideration when the solution pH is higher than ∼9 [41].

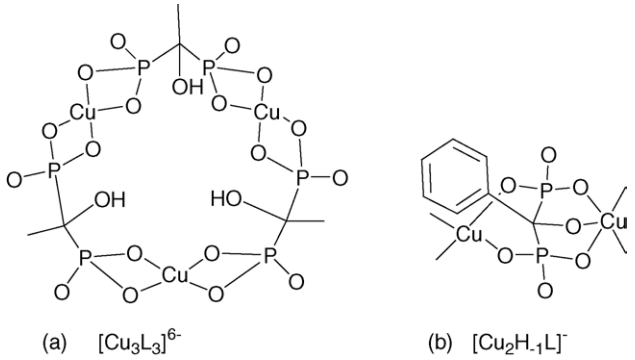

Scheme 3. The proposed solution structures for the oligomeric $[Cu_3L_3]^{6-}$ complex of **2** (a) and for the $[Cu_2H_{-1}L]^-$ complex of 1-phenyl-1-hydroxymethanediphosphonic acid (b).

$[Cu_2L]$ and $[Cu_2H_{-1}L]^-$ were also detected with the use of potentiometry and EPR methods in systems containing alkyl and aryl substituted derivatives of **2**, but never as the predominating species [42,43]. The ligand in the $[Cu_2H_{-1}L]^-$ complex was assumed to adopt the bis-bidentate binding mode with an alcoholic group coordinated in a deprotonated form (Scheme 3b). Studies of Al^{3+} and Fe^{3+} systems with aryl derivatives of **2** revealed that only mononuclear complexes are formed in the presence of Al^{3+}, while the replacement of Al^{3+} with Fe^{3+} ions resulted in the predominance of the $[Fe_2H_{-1}L_2]^{3-}$ complex over the whole pH range [44].

Table 1
Stability constants (log β) of $[ML]^{2-}$ complexes of **1** and **2** with several divalent metal ions

	Compound **1**		Compound **2**					
	0.1 M $NaClO_4$[a] [63]	0.5 M NaCl + Me_4NCl[a] [64]	0.15 M KCl[a] [65]	0.1 M KNO_3[a] [66]	0.1 M NH_4NO_3[a] [67]	0.2 M KCl[a] [41]	0.1 M KNO_3[a] [68]	0.1 M KNO_3[a] [69,70]
Fe^{2+}								12.9
Ni^{2+}				5.64			8.6	8.63
Cu^{2+}				6.38	11.84	12.70	11.9	12.0
Zn^{2+}				7.36			6.7	10.3
Cd^{2+}				5.98			8.7	8.7
Mg^{2+}	5.49		6.43					
Ca^{2+}			5.48					6.2
Be^{2+}		13.7						

[a] Medium.

Table 2
The coordination units and the superstructural motifs in the complexes of methane-1,1-diphosphonic acid

No.	Compound formula	Ref. code	Space group	Coordination unit	1D	2D	3D	Ref.
1-1	$[Co(NH_3)_4(H_2L)]$	BOBLAF	$P2_1/c$	(i)				[75]
1D coordination networks								
1-2	$Na_3[MgF(L)]\cdot H_2O$	DEKSIV	$P2_1/m$	(ii)	Motif (**a**)			[76]
1-3	$Na_3[Co(OH)L]$	DEKROA	$P2_1/m$	(ii)	Motif (**a**)			[76]
1-4	$NH_4[AlF(L)]$	GAMBAY	*Cmcm*	(ii)	Motif (**a**)			[77]
1-5	$(NH_4)_2[TiO(L)]$	GOMNEB	*Cmcm*	(ii)	Motif (**a**)			[78]
2D coordination networks								
1-6	$[Fe(H_2O)(HL)]_2\cdot 2H_2O$	QUAXPOU	$P\bar{1}$	Fe(1) (iii) Fe(2) (iii)	Motif (**b**)[a]	R4,8(16)		[79]
1-7	$Na_4[CoL]_2\cdot 2H_2O$	DEKSOB	$P2_12_12_1$	Co(1) (vi) Co(2) (vi)	Co(1) helix Co(2) helix	Motifs (**d′**) and (**b′**)[b] R3,6(12)		[76]
1-8	$Na_4[CuL]_2\cdot 2H_2O$	WUTMAZ	$P2_12_12_1$	Cu(1) (vi) Cu(2) (vi)	Cu(1) helix Cu(2) helix	Motifs (**d′**) and (**b′**)[b] R3,6(12)		[80]
1-9	$[Cu_3(H_2O)_2(HL)_2]\cdot H_2O$	WUTLUS	$C2/c$	Cu(1) (iv) Cu(2) (v)	Motif (**d**) Type (**e**)[a]	R4,8(16)[c] R4,8(16)[d]		[80]
1-10	$[Ni_4(H_2O)_3(L)_2]$	SIBLIY	Cc	Ni(1) (v) Ni(2) (v) Ni(3) (iv) Ni(4) (xxi)	Motif (**c**) Motif (**c**)	Motif (**e**) R4,8(16)[c] R3,6(16)	R4,8(16)[c]	[81]
3D coordination networks								
1-11	[ZrL]	XUWWAN	$P2_1$	(viii)	Zr helix		R3,6(14)	[82]
1-12	$Na_2[ZnL]\cdot 2H_2O$	VUZTOZ	$P2_12_12_1$	(ix)	Zn helices		R6,12(22)	[83]
1-13	$[Cu_2L]$	WUTLOM	*Pnma*	(vii)	Motifs (**d′** and **f**)		R4,5(10)	[84]
1-14	$[Ti_3O_2(H_2O)_2L_2]\cdot 2H_2O$	QUEJDIS	$P2_1/c$	Ti(1) (x) Ti(2) (ii)		Motifs (**d′** and **f**) Motif (**s**) R3,6(14) Joins T(1) 2D	R6,10(20)	[85]
1-15	$[Zn_4L_2]$	MULGUV	$C2/c$	M(1) (iv)		R4,8(16)[c]	R6,8(20)	[86]
1-16	$[Ni_4L_2]$	SIGQOO	$C2/c$	M(2) (iii) M(3) (ix)	Motif (**e**) Motif (**g**)	R2,4(12) Joins the monolayers		[81]
1-17	$[Zn_4(H_2O)_2L_2]$	MULGOP	$C2/c$	M(1) (iv)		R4,8(16)[c]	R6,8(20)	[86]
1-18	$[Ni_4(H_2O)_2L_2]$	SIBMOF	$C2/c$	M(2) (v) M(3) (ix)	Motif (**e**) Motif (**g**)	R2,4(12) Joins the monolayers		[81]

[a] Centrosymmetric dimer.
[b] Non-centrosymmetric dimer.
[c] Square grid.
[d] Corrugated 2D.

3.3. Delineation of the coordination networks in the complexes of methane-1-1-diphosphonic acid

The rigidity of **1** used as ligand at various protonation states, its size and geometry as well as the topology of the binding sites predispose for bidentate and bis-bidentate chelation as demonstrated in Table 2 which collects all the available metal complexes of **1**; coordination modes are shown in Scheme 4.

The vast majority of these compounds are catenated or polycatenated systems formed with variable metal ions or with the same metal ion, depending on the stoichiometry and the reaction conditions. There is a *plethora* of polymeric structural motifs observed in the complexes and to compare and characterize their infinite architecture is not a trivial task. One way to do this is to use the simplified Robson's method, considering the metal ion as a node and the ligand as a spacer. However, as already pointed out, the bidentate co-ordination is preferable in the studied systems and variable ring formations are ubiquitous in their extended frameworks. The supramolecular networks in these systems are also important in the structural description due to the predisposition of the ligand itself for hydrogen-bond formations, especially in low-dimensional coordination species. For that reason and for the purposes of this work we propose a notation, which is similar to that used for description of hydrogen-bonded networks [72,73]. The classification of the coordination frameworks in our method is based on the similarity of the ring motifs used to extend the individual coordination units in order to form 1D, 2D and 3D coordination frameworks. For identification of the coordination ring motifs we adopt the following description: *Rm,d*(*n*), where *m* means the number of metal centers in the ring, *d* the number of atoms donating electron pair to the metal center and *n* is the number of coordination and covalent bonds counted along the shortest path. This description is basically very

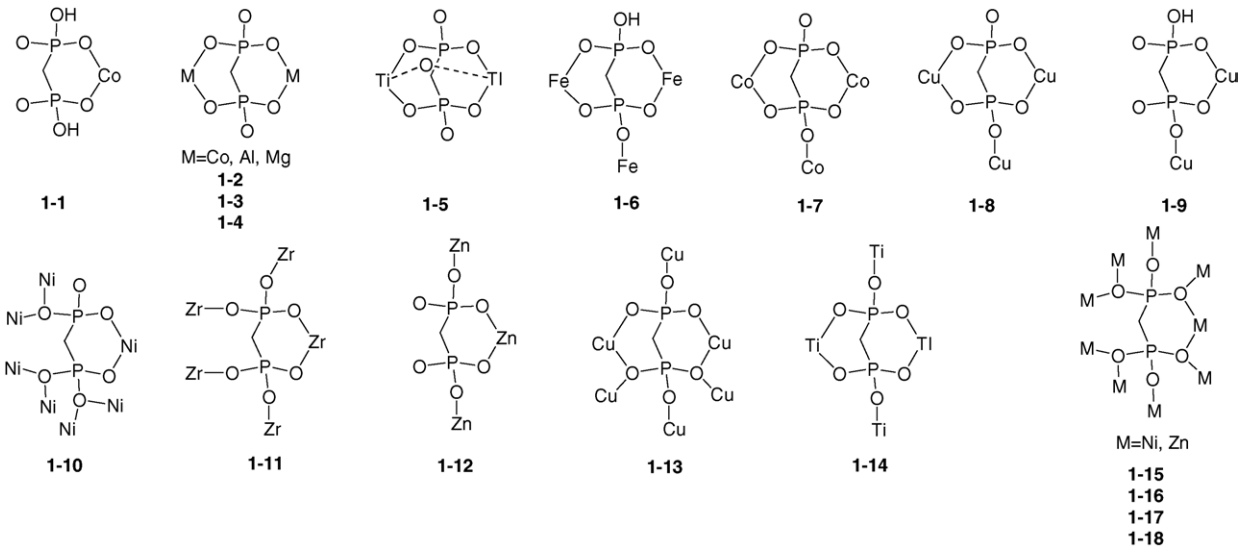

1-1 1-2 1-3 1-4 1-5 1-6 1-7 1-8 1-9 1-10 1-11 1-12 1-13 1-14 1-15 1-16 1-17 1-18

Scheme 4. Coordination modes of **1** in metal complexes **1-1** to **1-18**.

similar to that used for hydrogen-bonded ring motifs [74]. The proposed shorthand notation is advantageous in being informative about the size of the meshes and cavities, as well as about the phenomenon of catenation and the degree of catenation (DOC). Each point (atom) in the closed circuit has two connection bonds with the neighbors. So, the numbers of donating atoms in the ring is equal to twice the number of metal centers included in it. However, the number *d* becomes smaller if the coordination species is entangled or catenated and one or more donating atoms in the circle are shared.

3.3.1. Isolated coordination units

As can be seen from Table 2, all the compounds except for **1-1** [75] display high-dimensional coordination species in which the individual units cannot be separated without breaking coordination bonds. All possible coordination units observed for 4-, 5- and 6-coordinated metal ions are presented in Scheme 5.

From Schemes 4 and 5 it becomes obvious that in all cases the individual motif can be extended into higher dimensional coordination species. The only exception is **1-1**, in which the Co^{2+} coordinates one LH_2^{2-} and four neutral NH_3 ligands, type (i). The NH_3 sites introduce twelve additional hydrogen-bond donors to the system and dictate the supramolecular arrangement of the coordination units. Two very strong hydrogen bonds P(1)O–H···O=P(1) and P(2)O–H···O=P(2) organize the acid anions into monolayers with large meshes (R4,4(20)). The $Co^{2+}$and Cl^- ions and the NH_3 ligands protrude from these meshes and fall in the interlayer region. A very rich hydrogen-bonded network consisting of six N–H···Cl and seven N–H···O hydrogen bonds is traversing back and forth the neighboring inversion related layers in order to complete the final crystal structure.

3.3.2. One-dimensional coordination networks

Four complex salts **1-2** to **1-5** display identical 1D coordination arrays. The non-separable coordination units in them are very similar (type (ii)). Let us consider the 1D species in **1-2** [76] as presented in Fig. 2. The individual coordination unit is extended into a 1D species via a six membered R2,3(6) ring motif (motif (**a**), Scheme 6) comprising two metal centers and three donating atoms. One of the donating atoms in the 1D motif is X that serves to bridge the metal centers. The other two donating atoms are the oxygen atoms belonging to the same phosphonate group. Three hydrogen bonds donated from the water molecule towards a fluorine ion and one oxygen of the acid ligand organize the 1D coordination chains into thick molecular monolayers. The metal ions are arranged in the interior and oxygen sites on the surfaces of the layer. Three sodium ions coordinate the monolayers in order to form the crystal structure. Each of the sodium ions is five-coordinated with Na–O bonds from 2.29 to 2.5 Å. The 1D coordination unit of **1-3** [76] is the same as in **1-2** with the only difference that the bridging ligand is the hydroxyl group, which issues into a different supramolecular network. The crystals of **1-4** [77] and **1-5** [78] are isostructural. The 1D structural motif is R2,3(6). However, the ammonium ion in the last two compounds donating multiple hydrogen bonds

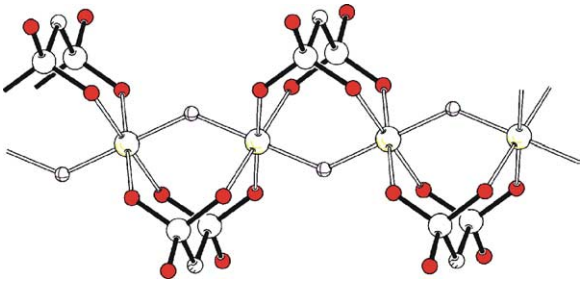

Fig. 2. The coordination chain in **1-2**.

Table 3
The coordination units and the superstructural motifs in the complexes of 1-hydroxyethane-1,1-diphosphonic acid

No.	Compound formula	Ref. code	Space group	Coordination unit	Linking motif			Ref.
Isolated mononuclear coordination units								
2-1	$K_4Na_2[CuL_2]\cdot 12H_2O$	DENXOJ	$P\bar{1}$	(xi)	Hydrogen-bonded ribbons, channel structure			[87]
2-2	$[Cu(H_3L)_2(H_2O)_2]\cdot 3H_2O$	NAWBES	$C2/c$	(ii)	Hydrogen-bonded porous 3D network			[88]
2-3	$(C_4H_{12}N)_2[Cu(H_2O)_2(H_2L)_2]$	NAVYOY	$P2_1/c$	(ii)				[89]
2-4	$(C_4H_{12}N)_2[Mg(H_2O)_2(H_2L)_2]$	FAPSIY	$P2_1/c$	(ii)	Hydrogen-bonded ribbons, hydrogen-bonded 3D network with channels along the ribbons where the amines are arranged			[90]
2-5	$(C_4H_{12}N)_2[Co(H_2O)_2(H_2L)_2]$	NAVYIS	$P2_1/c$	(ii)				[89]
2-6	$(C_4H_{12}N)_2[Zn(H_2O)_2(H_2L)_2]$	FAPTEV	$P2_1/c$	(ii)				[90]
2-7	$(C_6H_{16}O_3N)_2[Cu(H_2O)_2(H_2L)_2]$	HOCXEC	$P\bar{1}$	(xii)				[91]
2-8	$(C_6H_{16}O_3N)_2[Zn(H_2O)_2(H_2L)_2]$	FOVQAI	$P\bar{1}$	(xii)	3D hydrogen-bonded networks with channels where the amines are arranged			[92]
2-9	$(C_4H_{14}N_2)[Ni(H_2O)_2(H_2L)_2]$	SIGYIQ	$C2/c$	(xii)				[93]
2-10	$(NH_4)_2[(H_2O)_2Ni(H_2L)_2]$	FAPXID	$P2_1/c$	(xii)				[94]
Isolated coordination dimmers								
2-11	$K_4[Cu(H_2O)(H_2L)_2]_2\cdot 4H_2O$	HOWFEE	$P2_1/c$	(xiii)	Dimer motif of type (**h**)			[95]
2-12	$Cs_4[Cu(H_2O)(H_2L)_2]_2\cdot 4H_2O$	HOWHII	$P2_1/c$	(xiii)				[95]
2-13	$(CH_6N)_4[Cu(H_2O)(H_2L)_2]_2$	MANHAK	$P2_1/c$	(xiii)				[96]
2-14	$(C_3H_{12}N_2)_2[Ni((H_2O)(H_2L)_2]_2$	SIGSOQ	$P1$	(xiii)				[93]
1D coordination ribbons								
2-15	$[Cu(H_2L)(H_2O)]_2\cdot 7H_2O$	LOFGAO	Cc	(xiv)	Motif (**d′**)	Hydrogen-bonded monolayers via (P)OH···O(P)		[97]
2-16	$[Cu_3(H_2O)(HL)_2]\cdot 2H_2O$	WAJHIY	$P\bar{1}$	Cu(1) (xi)	R4,8(16)	Hydrogen-bonded 3D structure with hydrophilic channels and hydrofobic chambers		[98]
		WAJHIY01		Cu(2) (xv)				[99]
2-17	$[Cd(H_2L)]\cdot 2H_2O$	XISKOZ	$P2_1/n$	(xvi)	R2,3(6) motif (**o**)			[100]
2-18	$[Sr(H_2L)]\cdot 4H_2O$	VUJPOF	$C2/c$	(xviii)	R2,2(4) motif (**p**)	Hydrogen-bonded 3D network with water channels and hydrophobic chambers		[101]
2-19	$Na[CuCl(H_2L)]\cdot 3H_2O$	NAVYEO	$P2_1/c$	(ii)	Motif (**a**)	Hydrogen-bonded monolayers via (P)OH···O(P)	3D structure with hydrophilic channels and hydrophobic regions	[102]
2-20	$Rb(H_3O)[Cu(H_2L)_2]\cdot 2H_2O$	GOKVUX	$P\bar{1}$	(iv)	Motif (**j**) + hydrogen bonding	Hydrogen-bonded monolayers	Water hydrogen-bonded bridges	[103]
2-21	$(NH_4)_2[Cu(H_2L)_2]\cdot 2H_2O$	HOHPEZ	$P\bar{1}$	(iv)				[104]
2-22	$(NH_4)_2[Cu_3L_2(H_2O)_2]$	COYHAZ	$P2_1/n$	Cu(1) (xi)	R4,8(16) motif (**m**)	3D hydrogen-bonded structure with hydrophobic channels through the R4,8(16) ring and hydrophobic chambers between the ribbons		[105]
				Cu(2) (xv)				
2-23	$(C_3H_{12}N_2)[CuL]$	ICISUI	$C2/c$	(vi)	Alternating motifs (**k**) and (**l**)	3D hydrogen-bonded structure with channels via NH···O(P)		[106]
2-24	$(C_2H_{10}N_2)[CuL]$	ICISOC	$P2_1/n$	(vi)				[106]

2-25	$(C_2H_{10}N_2)[NiL_2]$	SiGQUU	C2/c	(iv)	Motif (**j**) + hydrogen bonding	Channels via $NH_3\cdots O(P)$		[93]
2-26	$(C_2H_{10}N_2)[Fe(H_2L)_2]\cdot 2H_2O$	UFITOS	*C*2/*c*	(iv)				[107]
2-27	$(C_2H_{10}N_2)[Zn(H_2L)_2]$	NEQDAO	*C*2/*c*	(iv)				[108]
2-28	$(C_4H_{14}N_2)[Mn(H_2L)_2]$	IGENUD	$P\bar{1}$	(iv)		Inter-chain POH$\cdots$O(P)	Channels 3D via POH$\cdots$O(P)	[109]
2-29	$(C_4H_{14}N_2)[Fe(HL)]_2\cdot 2H_2O$	CIRSUR	$P2_1/c$	(xvi)	R2,2(4) + R2,4(8)	POH$\cdots$O(P) inter-ribbon hydrogen bonding 3D hydrogen-bonded structure with amine templated channels		[110]
2-30	$(C_5H_{16}N_2)[Fe\ (HL)]_2\cdot 2H_2O$	UGINUT	$P2_1/c$	(xvi)	motifs (**k**″) + (**l**″)			[111]
2-31	$(C_4H_{14}N_2)[Zn(HL)]_2\cdot 2H_2O$	NEQDES	$P2_1/n$	(xvi)				[108]
2-32	$(C_5H_{16}N_2)[Zn(HL)]_2\cdot 2H_2O$	NEQDIW	$P2_1/n$	(xvi)	R2,2(4) + R2,4(8)			[108]
2-33	$(C_4H_{14}N_2)[Mn(HL)]_2\cdot 2H_2O$	IGEPAL	$P2_1/n$	(xvi)	motifs (**k**′) + (**l**′)			[109]
2-34	$(C_6H_{18}N_2)[Mn(HL)]_2\cdot 2H_2O$	IGEPIT	$P2_1/n$	(xvi)				[109]
2-35	$(C_5H_{16}N_2)[Mn_2(HL)_2]\cdot 2H_2O$	IGEPEP	$P2_1$	Mn(1) (xvi) Mn(2) (xvi)	Motifs (**k**″) and (**l**″) Lack of inversion center			[109]
2-36	$(C_6H_{18}N_2)[Zn_2(HL)_2]\cdot 2H_2O$	NEQDOC	$P\bar{1}$	Zn(1) (xvi) Zn(2) (ix)	Motifs (**k**) + (**l**) Zn(1) ribbons Motifs (**m**) + (**n**) in Zn(2) ribbons	Hydrogen-bonded monolayers pillared via amines		[108]
2-37	$(C_4H_{17}N_3)[Fe(HL)_2]\cdot H_2O$	UFITUY	*Pbcn*	(xvii)	Type (**j**′)	3D hydrogen-bonded porous structure with triamines clamping the ribbons		[107]
2D coordination frameworks								
2-38	$(C_4H_{14}N_2)[Cu_3(H_2O)_2L_2]$	COYLOR	$P\bar{1}$	Cu(1) (ii) Cu(2) (xix)	Joins the 1D rods of Cu(2) into square grid monolayer Motif (**r**)	Amines hydrogen bond neighboring monolayers		[105]
2-39	$(C_4H_{10}N_2)[Cu_3L_2]$	COYNIN	$P\bar{1}$	Cu(1) (xx) Cu(2) (xix)	Joins the Cu(2) rods into square grid monolayer Motif (**r**)	Amines stacked in channels		[105]
2-40	$(C_3H_{12}N_2)[Cu_3(H_2O)L_2]\cdot 2{,}5(H_2O)$	XONCUY	$P\bar{1}$	Cu(1) (xiv) Cu(2) (xix) Cu(3) (xix)	 Type (**r**) Type (**r**)	Joins 1D chains of Cu(2) and Cu(3) into square grid monolayer Amines are pillaring the layers		[112]
2-41	$[Pb(H_2L)]\cdot H_2O$	JEHLIR	$P2_1/c$	(xxi)	Monolayer			[113]
2-42	$[Ca(H_2O)_2(H_2L)]$	CAEADP	$P\bar{1}$	Bisdisphenoid	1D R2,2(4) 2D another R2,2(4)		3D structure via hydrogen bonds	[114]
3-1	$[Ca(H_2O)_5(H_2L)]$	CAVKUF	*Pnma*	Monocapped trigonal prism	Hydrogen-bonded 1D via $R_2^2(8)$			[115]

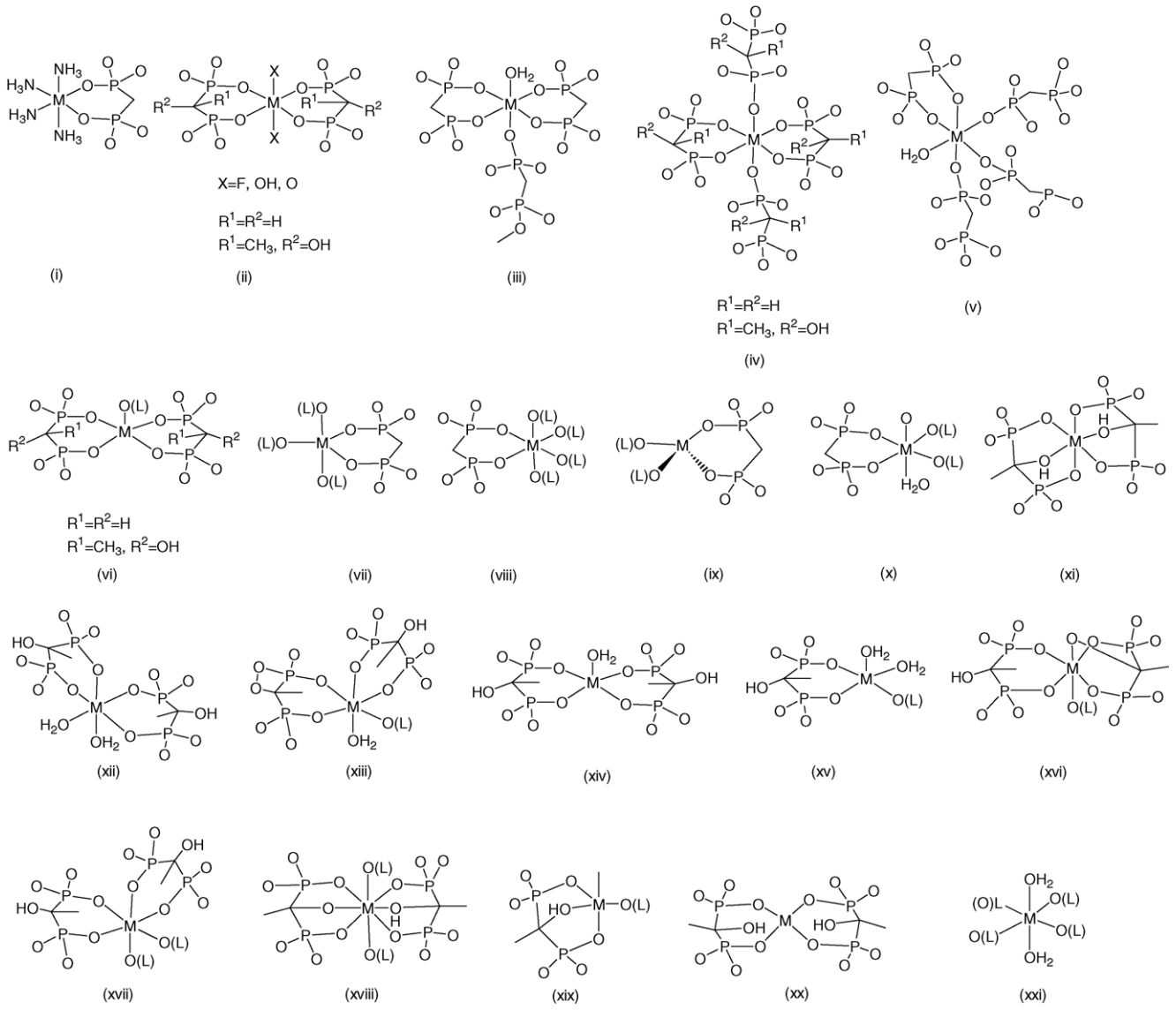

Scheme 5. The coordination units in metal complexes of **1** and **2**. Hydrogen atoms on the phosphonate groups, if any, are omitted for clarity.

towards the oxygen sites of the phosphonate ligands is responsible for the different organization of the coordination chains in the crystal structure.

3.3.3. Two-dimensional coordination networks

The vast majority of the metal complexes with **1**, form entangled 2D coordination networks. The simplest 2D coordination species is formed in **1-6** [79]. There are two crystallographically different Fe^{3+} ions with the same coordination mode (iii). Each of them coordinates three acid ligands HL^{3-} and a water molecule. Crystallographically independent coordination dimers formed via R2,4(8) motif of type (**b**′) are extended in two directions in order to form molecular monolayers via a big ring motif R4,8(16), where the two coordination waters reside (Fig. 3). The crystal water molecules are organized between the coordination layers and hydrogen bond them.

The complex salts **1-7** [76] and **1-8** [80] are isostructural with two symmetrically non-equivalent metal centers in the asymmetric unit. The crystal structure in these compounds is built up from undulate coordination monolayers. The sodium ions and the crystal water arranged in the interlayer region join the monolayers. The metal ions in them are five-coordinated with coordination unit of type (vi). The 2D coordination framework of the layers can be described as an arrangement of two different helical chains (the 1D coordination species of the two symmetry non-equivalent metal ions), that are multiple interlocked via R2,4(8) (motif **b**) in order to form undulate monolayers (Fig. 4). Cavities, encircled by 12-membered ring motifs R3,6(12), are generated between the loops of M(1) and M(2) helices. The charged phosphonate oxygen sites of the ligands (Scheme 4) are coordinated to the sodium ions and additionally hydrogen bonded to one of the water molecules. The second water molecule is only

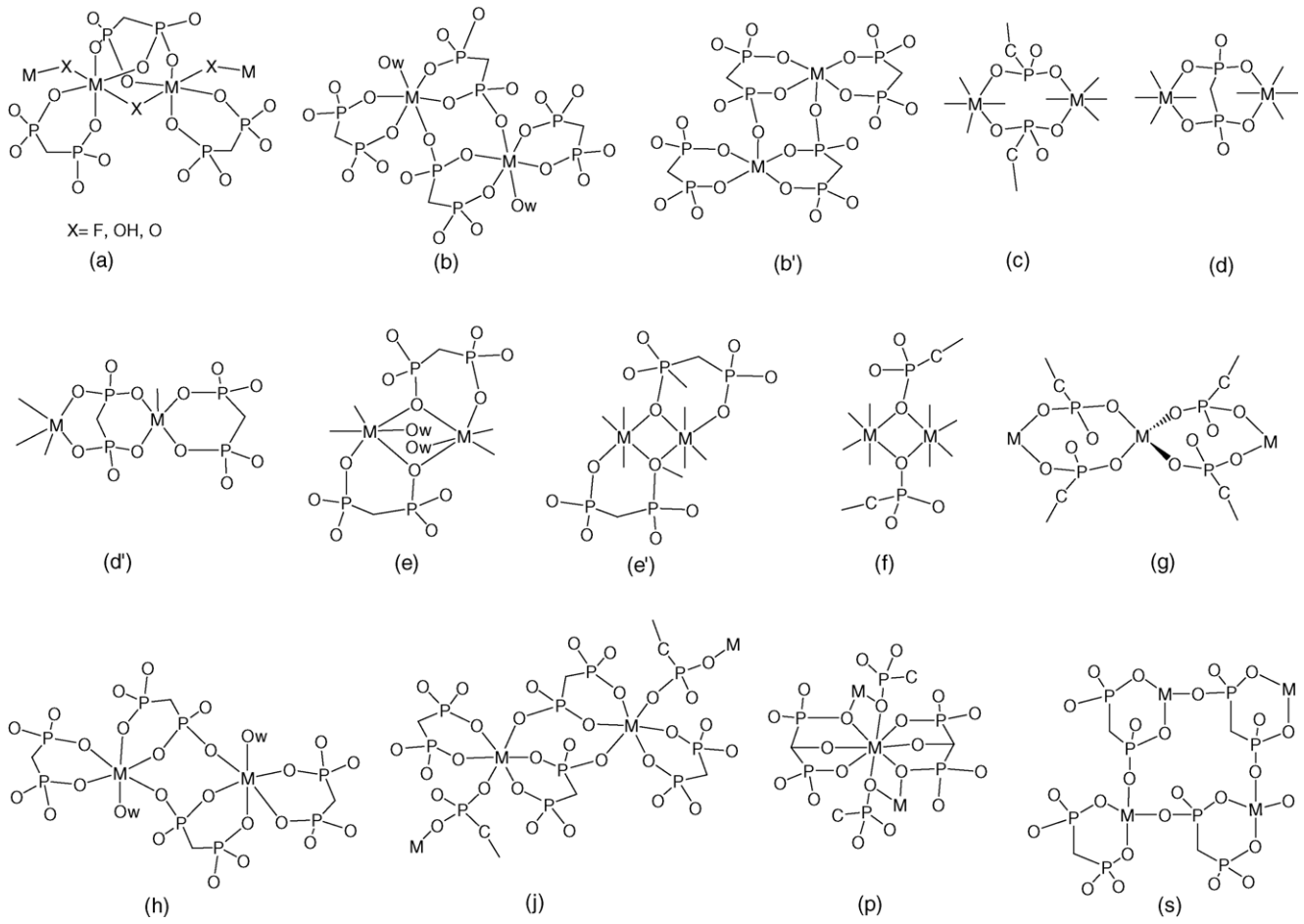

Scheme 6. Linking motifs in metal complexes of **1** and **2.** All hydrogen atoms are omitted for clarity, Ow corresponds to coordinated water.

used as a ligand site to the sodium ions, which are arranged in the cavities of the interlayer region.

The framework of the copper complex **1-9** [80] is quite different. One of the copper ions Cu(1) is symmetrically different and forms a square-grid 2D coordination framework with meshes characterized by the motif R4,8(16) (Fig. 5a). The other two Cu(2) ions are symmetrically identical and form dimers via a R2,2(4) ring motif of type (**f**) (Scheme 6). The Cu(2) dimers are extended via another R4,8(16) motif in order to form a corrugated 2D framework with large voids where the two coordination waters reside. The Cu(1) centers are arranged exactly in the middle of these voids and vice versa the dimer motifs R2,2(4) of the Cu(2) species are arranged exactly in the middle of the meshes of the Cu(1) network. The 2D species of Cu(1) and Cu(2) ions are polythreaded in order to form thick molecular monolayers (with thickness of ca. 6 Å), that can be considered as molecular polytubes with a diameter of ca. 3 Å (Fig. 5b). The Cu(1) are arranged in the middle of the interior. The monolayers are stacked one over the other in order to form a 3D structure with crystalline water molecules incorporated in the interlayer region (Fig. 5c). The protonated oxygen sites of the ligand, arranged outward from the monolayer donate two hydrogen bonds towards the crystal water and additionally accept a hydrogen bond from the coordinated water of the next monolayer. The coordinated water is arranged on the surfaces of the monolayer and forms both intra-layer and inter-layer hydrogen bonds.

The crystal net in the nickel complex **1-10** [81] is even more complicated. Thick monolayers are also issued from the polycatenation of polymeric species. There are four symmetry non-equivalent metal ions with different individual motifs: type (v) for Ni(1), Ni(2), type (iv) for Ni(3) and type (xxi) for Ni(4). Each of the ions Ni(1) and Ni(2) forms a polymeric coordination chain using the R2,4(8) motif. The 1D species of Ni(1) and Ni(2) are interweaved via R2,2(4) motif into a 2D framework with R4,8(16) meshes. Similar to **1-9**, Ni(3) ions form a square-grid 2D framework with meshes characterized by R4,8(16). The R2,2(4) ring motif interlocking Ni(1) and Ni(2) species is arranged in the middle of the R4,8(16) rings of the Ni(3) framework. Ni(4) ions form another 2D framework with T-shaped meshes characterized by R3,6(16) ring motif. The two frameworks of Ni(3) and Ni(4) are also interlocked via another R2,2(4) motif and additionally polythreaded by the 1D chains of Ni(1) and Ni(2) ions via two more R2,2(4) motifs in order to form very thick molecular

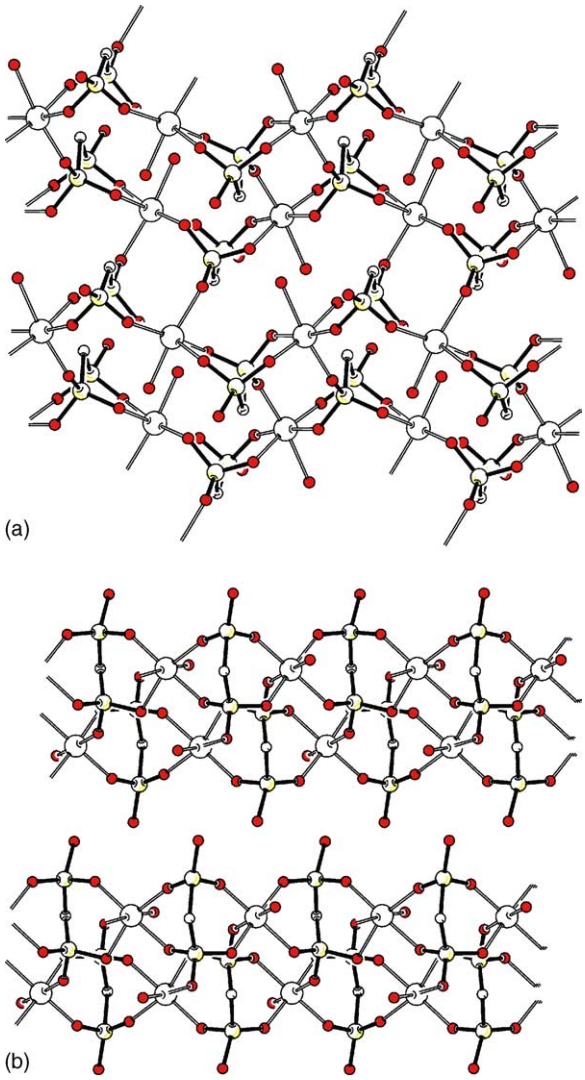

Fig. 3. A view of the monolayer (a); side view of two monolayers (b) in **1-6**.

monolayers. Hydrogen bonds donated from the coordination water join the monolayers into 3D supramolecular network.

3.3.4. Three-dimensional coordination frameworks

Eight complexes **1-11** to **1-18** were found to display entangled 3D structures. The simplest of them is **1-11** [82] with a non-separable coordination unit of type (viii). The 3D coordination framework can be deciphered as a parallel arrangement of helical chains along the *b*-axis, that are interlocked by the R2,4(8) motif (**d**) in order to form entangled 3D framework with large cavities closed between the helical grooves. The shortest closed circuit, incorporating three metal centers is characterized with a R3,6(14) ring motif (Fig. 6). The four-coordinated central ion in **1-12** [83] is tetrahedral with a coordination unit of type (ix). Similar to **1-11**, the 3D structure in this crystal can be considered as an interweavement of helical chains, formed by one chelate and one single bonding and interlocked via the other single bonding in order to form a 3D coordination framework with very large cavities, where

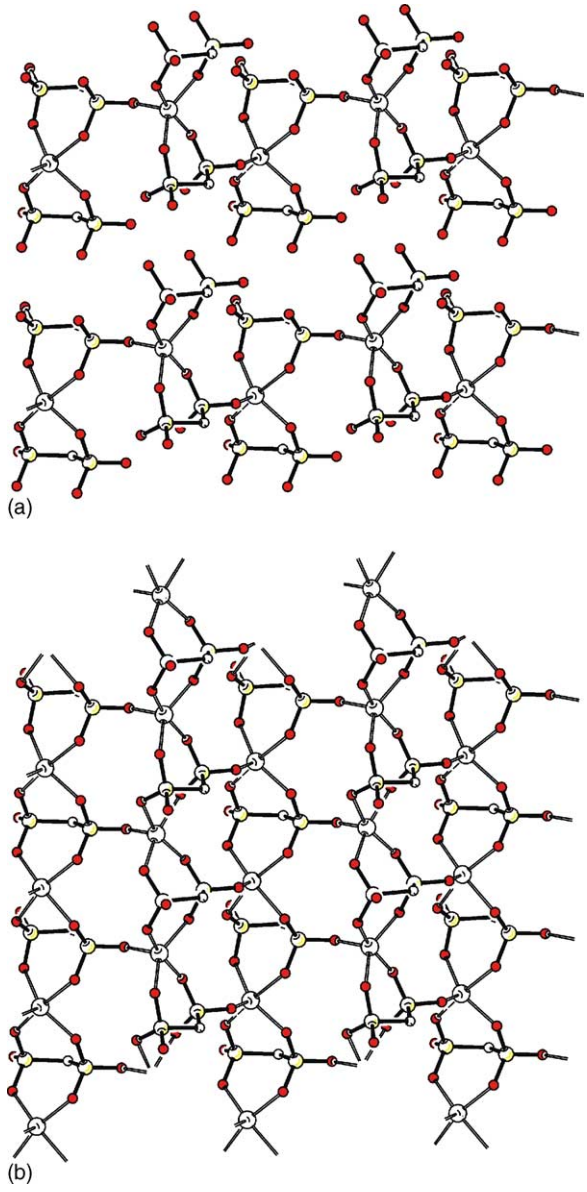

Fig. 4. Two translation related helical chains of Co(1) (a) and the monolayer formed by interweaved Co(1) and Co(2) helices (b) in **1-7**.

crystal water is incorporated. The shortest circuit in this structure is closed between six metal centers generating R6,12(22) ring motifs. The central ion in the copper complex **1-13** [84] is five-coordinated with a trigonal bipyramidal individual unit of type (vii). The 3D coordination framework can be considered as interpenetration of undulate coordination layers (Fig. 7). The interlocking motif is R2,2(4) and the shortest circuit incorporating three metal ions of the 3D coordination species is R4,5(10).

There are two crystallographically different metal centers in **1-14** [85]: Ti(1) and Ti(2) with coordination units of types (x) and (ii), respectively. The Ti(2) ions occupy special positions in the inversion center. The Ti(1) ions display 2D coordination species and form molecular sheets with R3,6(14) meshes. The Ti(2) ions are arranged between the inversion

related sheets and serve to join them via R2,3(6) motifs in order to form a porous 3D framework. Large hydrophilic cavities with R6,10(20) ring motif are generated in the inter-layer region, where both the coordinated and the crystal water molecules are arranged, additionally joining the monolayers via five different hydrogen bonds.

Four complexes **1-15** to **1-18** [81,86] are isomorphic and display identical 2D entanglement. For that reason we will make a structural analysis only for one representative. In **1-15** there are three symmetry different metal ions, with different coordination units: type (iv) for Zn(1), type (iii) for Zn(2) and type (ix) for Zn(3). Similar to the copper complex **1-9** the 2D coordination species formed by Zn(1) and Zn(2) are interweaved in order to form a monolayer (polytubes).

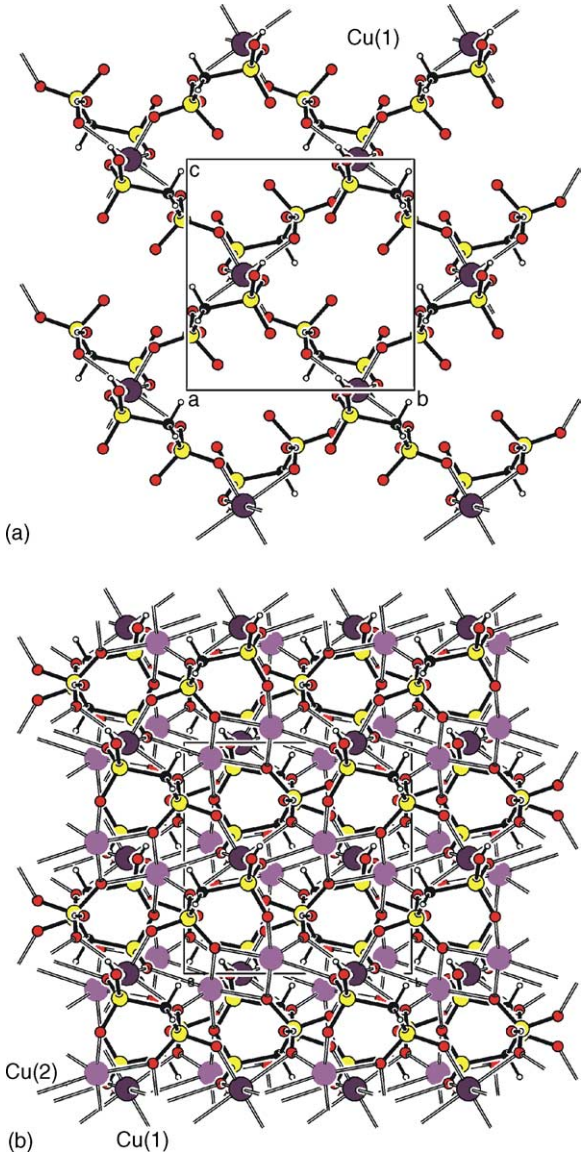

Fig. 5. The square-grid 2D framework of Cu(1) (a); a view of the monolayer: 2D polytubes issued from the interpenetrated 2D of Cu(1) and Cu(2) (b); inter-layer relationships (c) (the bridging water hydrogen bonds are omitted for clarity) in **1-9**.

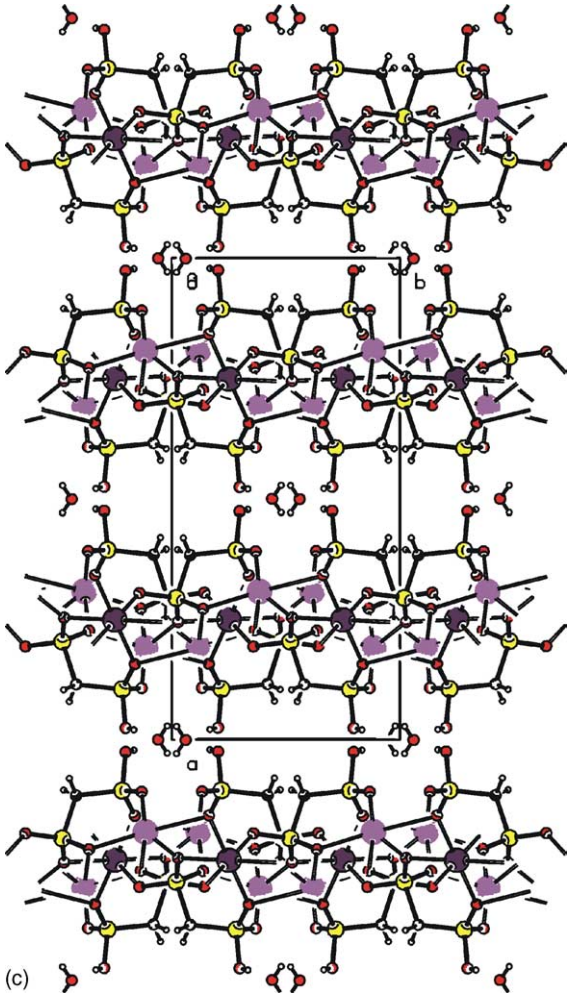

Fig. 5. (*Continued*).

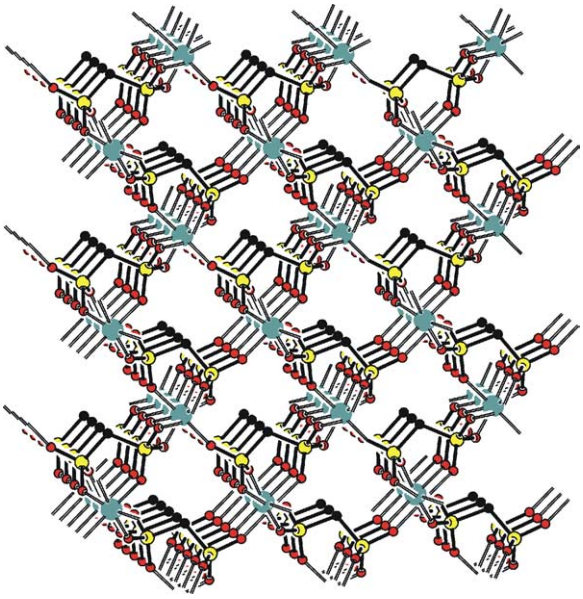

Fig. 6. The porous 3D framework in **1-11**.

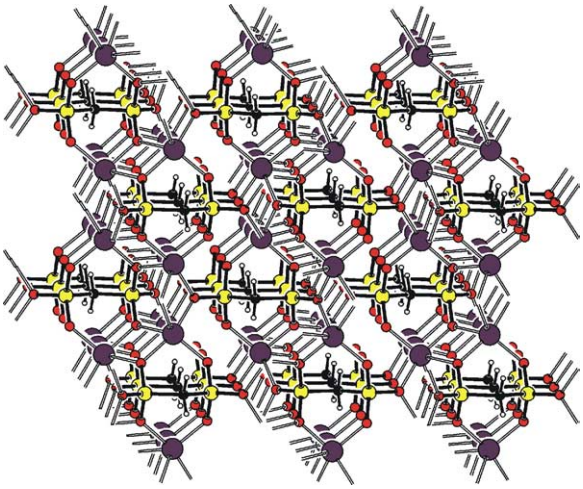

Fig. 7. The porous 3D framework in **1-13**.

However, unlike the copper complex, where the monolayers were hydrogen-bonded in order to form a 3D supramolecular network, the tetrahedral Zn(3) ions are arranged between the monolayers and extended (via R2,4(6) motif) into 1D polymeric chains, that interweave the monolayers in order to form a polythreaded 3D coordination framework with large cavities. The polythreading between the 2D species of Zn(1) and Zn(3) as well as between those of Zn(2) and Zn(3) takes place via the same R2,3(6) ring motif and smallest ring motif encompassing three different zinc ions is R6,8(20) (Fig. 8). These symbols already advise us of polycatenation phenomena, since the number of donating atoms in them is smaller than twice the number of metal centers. The only difference between **1-15** and **1-17** is the presence of coordinated water in the latter with Zn(2) coordination unit of type (v), which does not play any significant role for the 3D interweavement since the water molecules are projecting from the exterior of the monolayer.

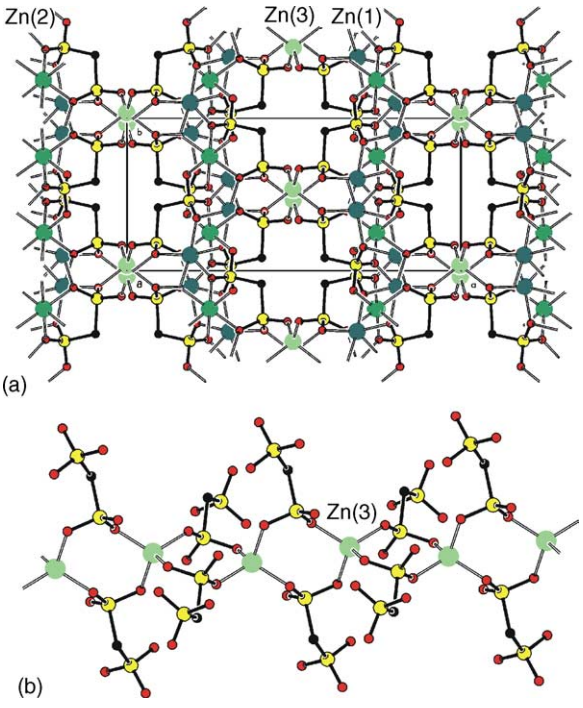

Fig. 8. The porous 3D issued from the interweavement of Zn(1), Zn(2) and Zn(3) polymeric species (a); 1D polymeric chain of Zn(3) threading the monolayers with (**g**) motif indicated (b) in **1-15**.

3.4. Delineation of the coordination networks in the complexes of 1-hydroxyethane-1,1-diphosphonic acid

The presence of an additional electron donating site on the hydroxylic group enables a tridentate binding of **2** with resultant significantly modified coordination abilities (Table 3). On the other hand the hydroxyl group can serve both as hydrogen-bond donor and acceptor, so even in systems with fully deprotonated phosphonic groups of **2**, hydrogen-bond formations are still possible. New coordination modes and structural motifs extending them in 1D and 2D have been found. The observed binding patterns of **2** are collected in Scheme 7. The coordination units and the extending motifs are presented in Schemes 5 and 6.

3.4.1. Isolated mono- and dinuclear coordination units

Ten compounds **2-1** to **2-10** [87–94] were found to display isolated 0D coordination units extended into supramolecular networks by hydrogen bonds. A tridentate metal binding of the acid ligand is observed in **2-1**. The coordination unit, assigned as type (xi), is extended into 1D ribbons via a hydrogen bond executed between the OH-group and the phosphonate oxygen site. The sodium ions join the ribbons into formal monolayers and the potassium ions join the monolayers in 3D. The crystal water molecules are arranged between the formal monolayers and form an extended hydrogen-bonded network stabilizing the crystal structure. In the complex **2-2** the coordination unit (type (ii)) is extended via phosphonic–phosphonate and hydroxy–phsphonic hydrogen bonds in order to form porous 3D supramolecular network. Both, the coordinated and the crystal water molecules are arranged in the big cavities (size of 7.5 Å × 5.7 Å × 6.3 Å) of the network. The bis(diethyl)ammonium metal diphosphonates **2-3** to **2-6** are also characterized by the (ii) type 0D unit. A very strong phosphonate–phosphonate hydrogen-bond joins neighboring inversion related coordination units into molecular ribbons along the *a*-crystallographic axis. Each ribbon is linked via another phosphonate–phosphonate hydrogen-bond with four neighboring ribbons (*c*-glide relationship) in order to form a channeled 3D structure (Fig. 9a) The channels are parallel to the molecular ribbons and characterized with a 28-membered hydrogen-bonded ring motif $R_6^6(28)$ (Fig. 9b). The bis(diethyl)ammonium ions are arranged along the channels and serve to template them. The methyl groups of the ligands also fall in the channels. All four compounds are isomorphic with $P2_1/c$ space group. The compounds **2-7** to **2-10** display an identical coordination unit of type (xii), organized via hydrogen-bonds in order to

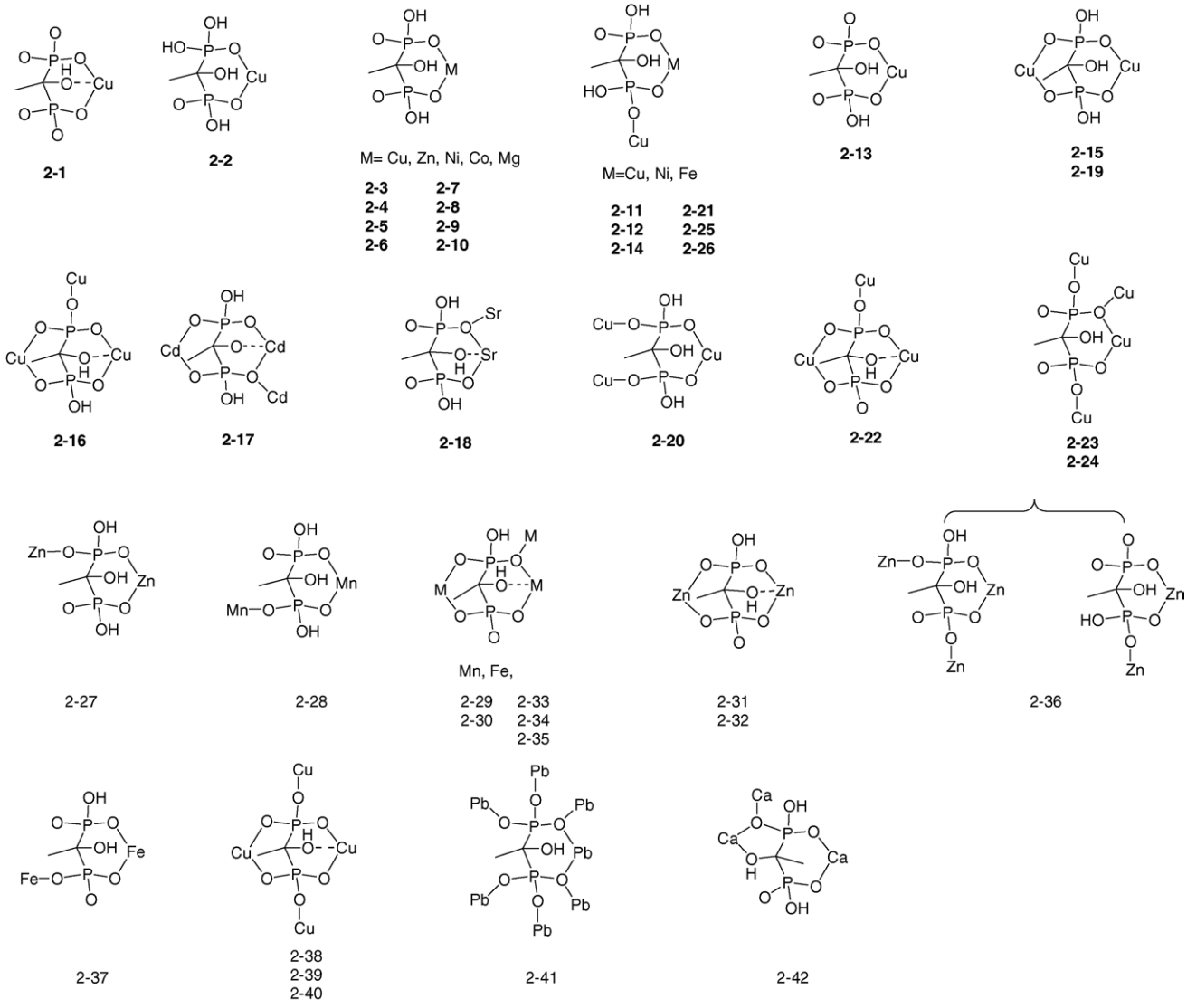

Scheme 7. Coordination modes of **2** in metal complexes **2-1** to **2-42**.

form ammonium templated channel structures. However, the size and the shape of the channels in them depend upon the size and the shape of the organic amine (Fig. 10). On the other hand, four compounds **2-11** to **2-14** [93,95,96] were found to display isolated coordination dimers of type (**h**). The dimer units, stabilized by several intra-dimer hydrogen bonds, are extended via an inter-dimer hydrogen-bonded ring motif $R_2^2(12)$ in order to form 1D ribbons along the *a*-direction. Strong phosphonate–phosphonate hydrogen bonds join the neighboring ribbons furnishing a crystal network with channels generated between each four ribbons (see Fig. 11), where the cations or the amines are arranged.

3.4.2. One-dimensional coordination networks

Twenty-three complexes of **2** were found to form 1D coordination species that are further extended into higher networks via hydrogen bonds. A big structural diversity is observed already on the level of the basic coordination units and the extending motifs as well as on the supramolecular level. Along with the coordination geometry and the ability of the metal ion, the specificity of the basic coordination unit and the topochemical predisposition for hydrogen-bond formation, the nature of the counter-ion(s) may play a role for the packing preferences of the coordination species. Since metal diphosphonates templated with organic amines predominate in this group, the size of the amine apparently influences the anionic network and hence the environment of the central atom. All these factors are discussed in the original papers and hereafter we address exclusively the topological similarities/dissimilarities of the coordination species and consider the differences in the supramolecular networks.

The geometry of the copper ions in **2-15** [97] is square pyramidal. There are two crystallographically distinct metal centers with the same coordination unit (xiv), that is extended into 1D coordination chain via a (**d′**) motif. (P)O–H···O(P) hydrogen bonds are used to arrange the chains into mono-

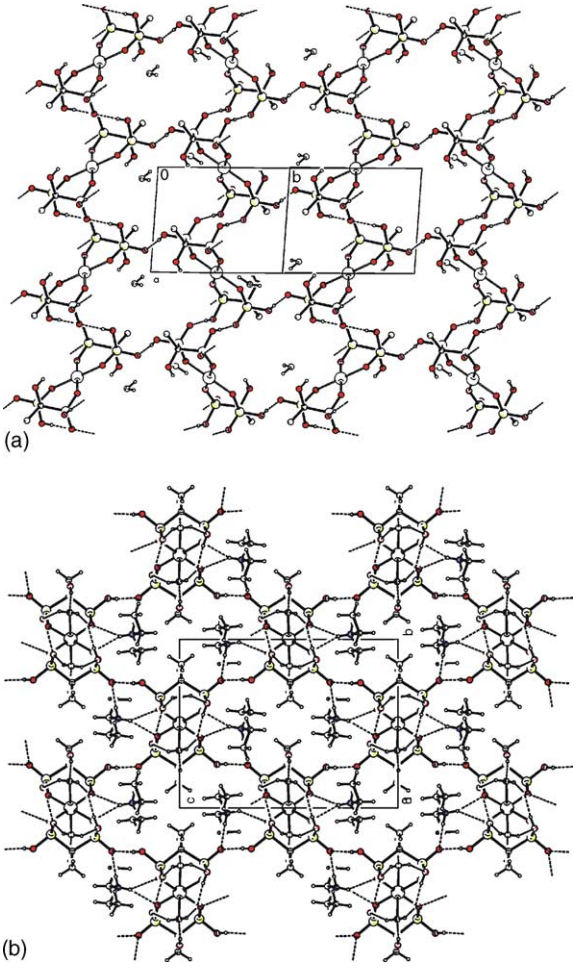

Fig. 9. The supramolecular network (a); the channels with the amines (b) in **2-3** to **2-6**.

layers with rectangular windows. The coordinated water molecule donates hydrogen bonds towards the neighbouring layer completing the 3D network. The crystal water is arranged between the layers and forms an extended hydrogen-bond networks. The metal ions in **2-16** [98,99] display two different coordination geometries: octahedral and square pyramidal. The one-dimensional interplay formed by two different coordination units of type (xi) for Cu(1) and type (xv) for Cu(2) is unique, not observed in other compounds (see Fig. 12a). Each Cu(2) unit bridges two Cu(1) units and each Cu(1) unit bridges four Cu(2) units. The extension motif is R4,8(16). The 1D coordination species can be considered as 1D coordination rod with Cu(1) arranged in the interior and Cu(2) on the surface or as thick ribbon formed from two inversion related Cu(2) chains joined via Cu(1) (see Fig. 12b). The latter description is more appropriate considering the hydrogen bonds along the chains and between the chains. For packing reasons no direct inter-ribbon phosphonate–phosphonate interactions are possible and the ribbons are hydrogen-bonded in 3D by the crystal water. The coordination water molecules reside in the hydrophophilic channels running through the meshes. The

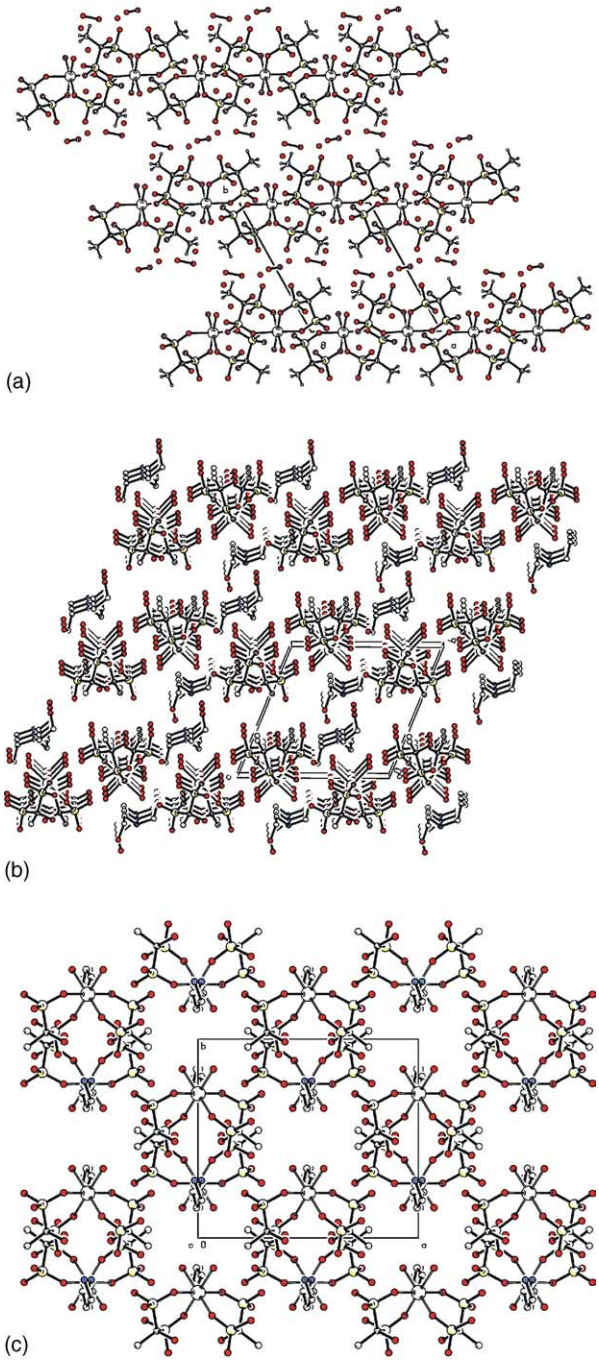

Fig. 10. The hydrogen-bonded chains in **2-7** to **2-10** (a); the channels in **2-8** (b); the channels in **2-9** (c). The hydrogen bonds are omitted.

methyl groups are arranged in hydrophobic chambers generated between the ribbons.

The 1D species in **2-17** [100] can be considered as an interweavement of two identical coordination chains in order to form a molecular ribbon. The coordination unit is (xvi) and the interlocking motif (**o**) (Fig. 13). The shortest ring motif including two metal centers is R2,3(6). The ribbon arrangement is similar to that in **2-16**. However, due to the different intra-ribbon relationships the compound crystallizes

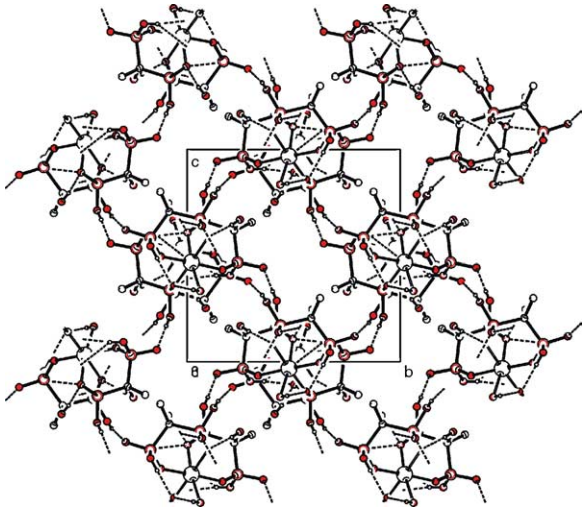

Fig. 11. A view along the channels in **2**-**11**.

with the orthorhombic $P2_1/n$ space group. The Sr^{4+} ions in **2**-**18** [101] are surrounded by four ligands forming an eight-coordinated unit (xviii) with two significantly longer and two significantly shorter Sr–O bonds. The intermediate coordination bonds are almost coplanar. The coordination unit is extended via a R2,2(4) motif (**p**) formed by the shortest and the longest bonds in order to form 1D cylindrical rods with the metal ions arranged along its axis and ligand anions arranged on its surface. Very strong (P)O–H···O(P) and (C)O–H···O(P) hydrogen-bonds strengthen the rod surface. The water molecules are arranged in channels between the coordination rods and bridge them via Ow–H···O(P) and (P)O–H···Ow hydrogen bonds. The methyl groups are occupying the hydrophobic chambers formed between the coordination rods.

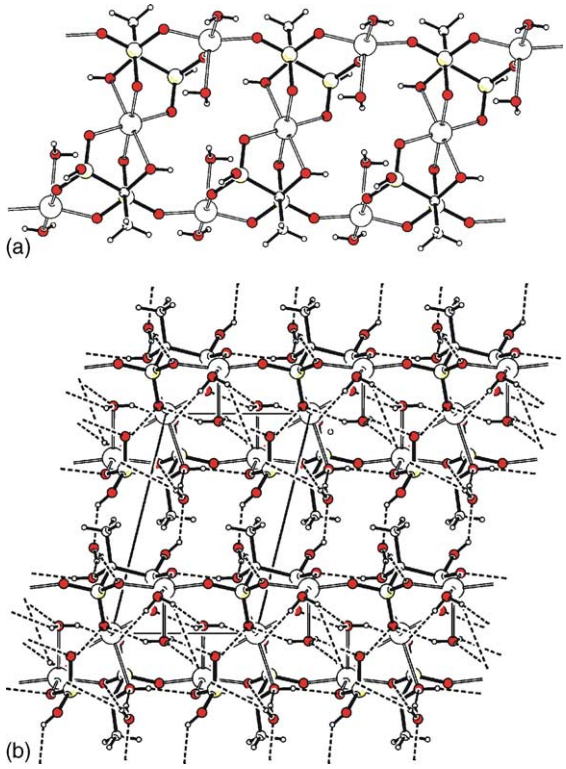

Fig. 12. The1D ribbon formed by Cu(1) and Cu(2) (a); inter-ribbon space (b) in **2**-**16**.

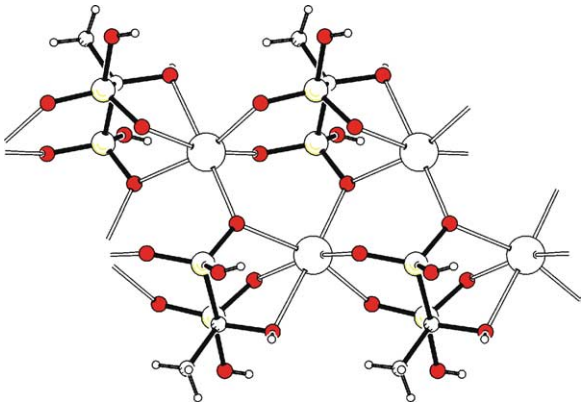

Fig. 13. The interlocking motif (**o**) in **2**-**17**.

In **2**-**19** [102] the chlorine ion bridges two neighboring metal centers. The coordination units (ii) and the extension motif (**a**) are the same as in **1**-**2**, **1**-**3**, **1**-**4** and **1**-**5**. The coordination chains are arranged into meshed monolayers via (P)O–H···O(P) hydrogen bonds. The meshes of neighboring monolayers are stacked one over the other in order to form hydrophilic channels, where the sodium ions and the three crystal water molecules reside. Two of the water molecules situated close to the monolayer surfaces, serve as donating sites to the sodium ions. The third one is at a middle distance between the monolayers. The methyl groups, protruding from the monolayers, also fall in the interlayer region. So, hydrophobic and hydrophilic regions are generated in the interior between the monolayers. In **2**-**20** [103], the basic coordination units are of type (iv) and the motif (**j**) is used for their extension into 1D ribbons. The hydrogen-bond interactions established between the hydronium ion and the anionic network organize the ribbons into monolayers. The rubidium cations are also arranged in the monolayer. The crystal water molecules incorporated between the layers hydrogen-bond them. The ammonium analogue **2**-**21** [104] presents an identical 1D coordination species as **2**-**20** and both crystals are isomorphic with $P\bar{1}$ space group. However, some differences are observed in their hydrogen-bonded networks.

The coordination units (xi and xv) and the 1D motif R4,8(16) in **2**-**22** [105] are the same as in **2**-**16**. However, the tetrahedral configuration of the ammonium ion and its hydrogen-bond donor capabilities enforce different 3D organizations with the $P2_1/n$ space group. The ammonium ions reside in the hydrophilic channels closed between the 1D coordination ribbons. The geometry of the Cu-center in 1,2-propanediammonium and ethylenediammonium salts **2**-**23**, **2**-**24** [106] is square pyramidal with coordination units (vi). Both compounds display identical polymeric chains, formed

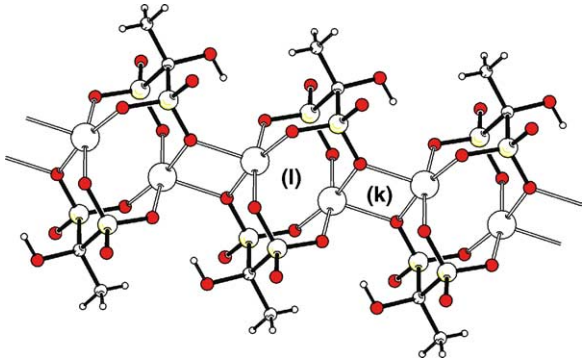

Fig. 14. The 1D polymeric chain in **2-24** with interlocking (**k**) and (**l**) motifs.

by alternating motifs (**k**) and (**l**) (Fig. 14) and arranged into channel structures. Even so, the 3D supramolecular networks in them are different due to geometrical differences of the templates.

The polymeric ribbons in **2-25** to **2-28** [93,107–109] are identical to those observed in **2-20** and **2-21**, formed from coordination units (iv) via the motif (**j**). In compounds **2-25** to **2-27**, strong (P)O–H···O(P) and (C)O–H···O(P) hydrogen bonds are established along the ribbons. The amines, arranged along the ribbons are cross-linking them via three hydrogen bonds. Hydrophilic and hydrophobic regions are

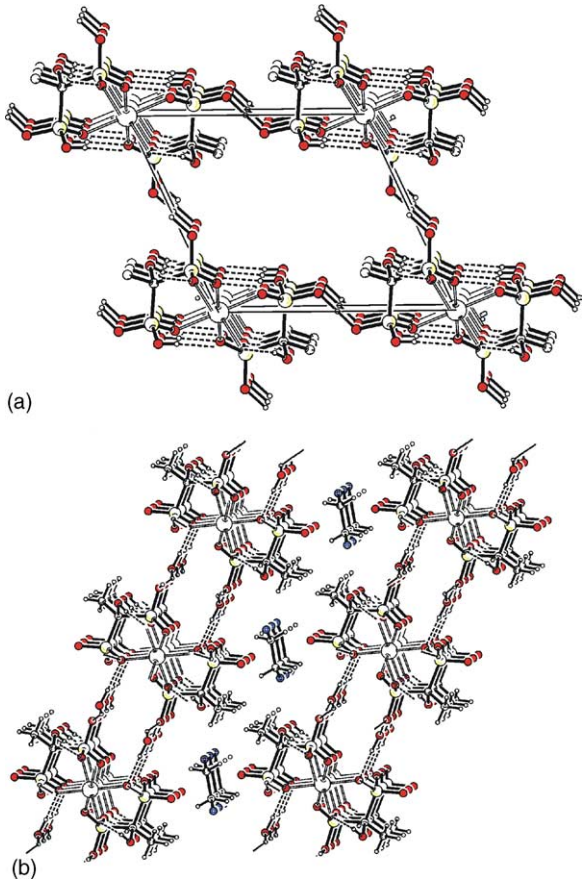

Fig. 15. A view of the channel in **2-28** (a); the amines across the channels in **2-27** (b).

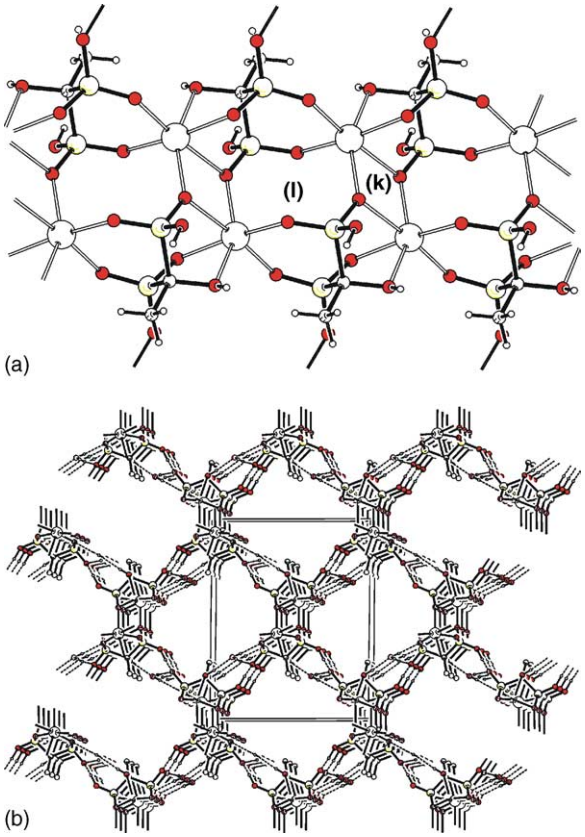

Fig. 16. The 1D polymeric chain (a); the channels (b) in **2-34**.

generated in the interribon region, where the crystal water and the methyl groups of the ligands reside (Fig. 15a and b).

On the other hand, the size of the amine enforces a quite different supramolecular organization in **2-28**. The ribbons in this compound are interconnected via a very strong interribbon (P)O–H···O=P hydrogen bond in order to form a structure with big channels (of size of ca. 16.6 Å × 10.6 Å) (Fig. 15a). The diamines are arranged across the channels and serve to template them.

Six compounds **2-29** to **2-34** [108–111] display the same coordination units. The octahedral geometry of the metal ion in them is strongly distorted. The basic unit (xvi) is polymerized via a centrosymmetric R2,2(4) motif of type (**l′**) in order to form coordination ribbons similar to that in **2-23** and **2-24** (Fig. 16a). The extension motifs (**k′**) and (**l′**) are similar to that in **2-23**, **2-24**, but not the same. The strong (P)O–H···O(P) hydrogen bonds also join the ribbons closing big channels templated by the amines (Fig. 16b). The influence of the long organic amine on the coordination geometry of the metal ion and, therefore, on the crystal packing is evident in the compounds **2-35** [109] and **2-36** [108]. Although the two metal centers in **2-35** have identical coordination units (xvi), their environments are slightly different which destroys the inversion relationship in the polymerizing motif and the compound crystallizes with the polar $P2_1$ space group. Compound **2-36** forms a completely different

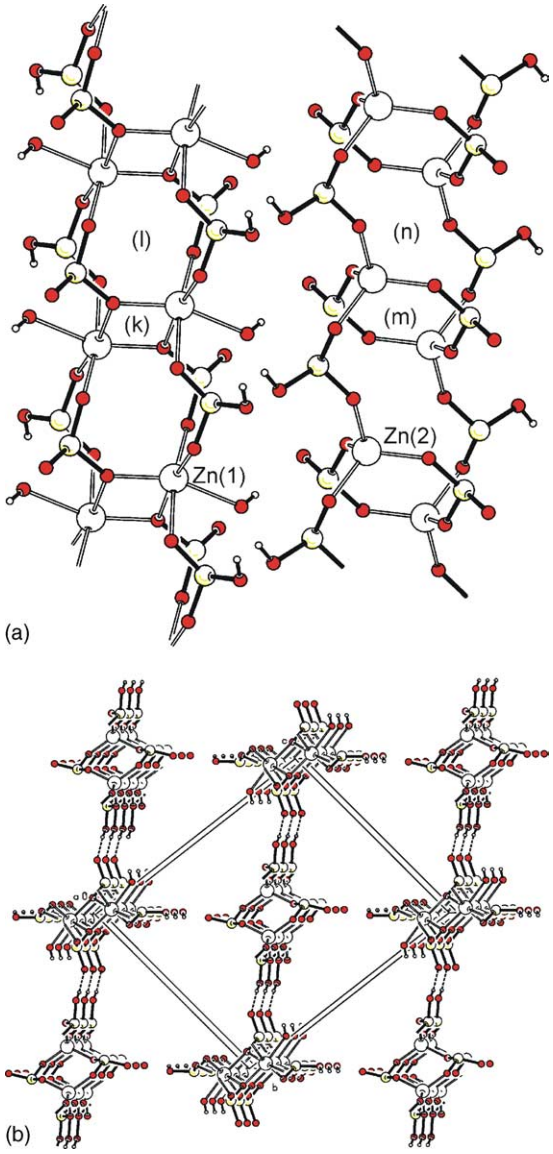

Fig. 17. 1D coordination ribbons of Zn(1) and Zn(2) (a); the channels (b) in **2-36**.

structure. The two metal ions, displaying coordination units of the type (xvi) for Zn(1) and (ix) for Zn(2), form two different, parallelly arranged 1D coordination ribbons. Alternating motifs (**k**) and (**l**) are used in the Zn(1) ribbons and motifs (**m**) and (**n**) in Zn(2) ribbons (see Fig. 17a). Two different rings R2,2(4) and R2,4(8) are generated in the Zn(1) ribbon and two more rings R2,4(8) and R2,4(12) in the Zn(2) ribbon. Two strong (C)O–H···O(P) hydrogen bonds join the ribbons in 2D monolayers, that are bridged via the water molecules in 3D network containing two kinds of cavities (Fig. 17b). The 1,6-hexamethylenediammonium ions fill in the cavities and serve to pillar the monolayers via extensive N–H···O cationic–anionic interactions. The coordination ribbons in **2-37** [107] are formed from coordination units of type (xvii), extended via a motif (**j′**). The wavy ribbons are arranged along the *b*-axis and clamped by the long diethylenetriammonium

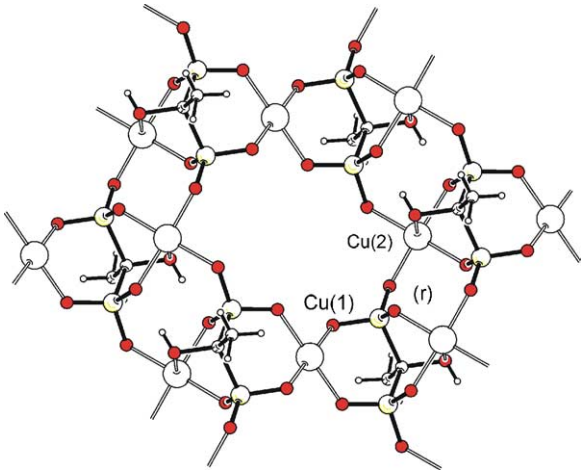

Fig. 18. The square-grid 2D framework of Cu(1) and Cu(2) in **2-39** with interlocking (**r**) motif.

ions in order to generate 3D with cavities. There are no direct interactions between the ribbons.

3.4.3. Two-dimensional coordination networks

Only five complexes are found to form 2D coordination frameworks. There is no single complex with a 3D coordination framework. The three copper complex salts **2-38** [105], **2-39** [105] and **2-40** [112], incorporating different organic diammonium cations, are isostructural. In all of them there are two crystallographically distinguishable copper ions: one of them is extended into 1D coordination polymers and the other connects the chains in order to form square grid monolayers with large meshes of R4,8(16). Compounds **2-38** and **2-39** display identical Cu(2) coordination units of type (xix) extended into 1D via a (**r**) motif (Fig. 18). However, the geometry of the Cu(1) ion that joins the chains is different: octahedral in **2-38** and planar in **2-39**. So, the Cu(1) coordination units are of type (ii) and (xx), respectively. The amines are differently arranged in the channels through the meshes of the monolayers. For example, the piperazinium ions in **2-39** are stacked over one another in the channels and the ethane-1,4-diammonium ions in **2-38** hydrogen-bond the neighboring monolayers. On the other side, all three copper ions in **2-40** [112] are crystallographically distinguishable, with (xix) type coordination units for Cu(2) and Cu(3) and (xiv) unit for Cu(1). Cu(2) and Cu(3) form two polymeric chains using the same (**r**) motif and Cu(1) joins the chains in square-grid monolayers with R4,8(16) meshes (Fig. 19). The coordinated water and the methyl groups protrude from the monolayers and sit in the interlayer region. The propane-1,3-diammonium ions are arranged along the channels through the meshes and serve to pillar the layers forming an extensive N–H···O network.

The trigonal bipyramidal coordination unit of type (xxi) in **2-41** [113] is extended via R2,2(4) motifs in order to form helical chains along the *b*-axis. In fact, the 1D polymers are consisting of edge-shared trigonal pyramides. The molecular monolayers issue from the interweavement of neighboring

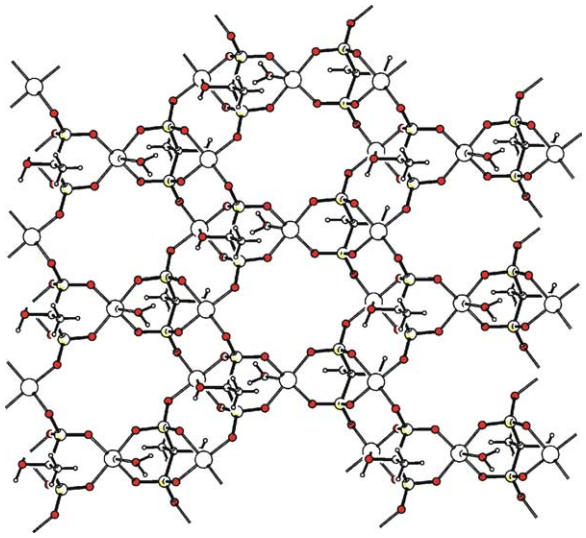

Fig. 19. The square-grid monolayer in **2**-**40**.

opposite running helices. The interlocking motif between the helices R2,4(8) is shown in Fig. 20. The crystal water is arranged between the monolayers and hydrogen-bonds them.

The irregular eight-fold geometry is not surprising for the relatively big calcium ion. In **2**-**42** [114] Ca^{2+} is in a strongly distorted bisdisphenoidal environment of eight oxygen sites belonging to three different ligand moieties and three water molecules. Two kinds of chelate rings are formed with two inversion-related anionic portion: one six-membered ring and one five-membered ring. Inversion related coordination units are extended via alternating R2,2(4) and R2,4(8) ring motifs into 1D polymeric formation. One of the coordinated water molecules joins the inversion related 1D ribbons via another R2,2(4) ring motif in order to form (0 0 1) monolayers (Fig. 21). The other coordinated water protrudes from the windows and serves exclusively to link the neighboring layers via O–H· · ·O(P). An extensive intra-layer hydrogen-bond network is also established. The shortest Ca–Ca distances are: 3.82 Å along the ribbons, 4.12 Å between the ribbons and

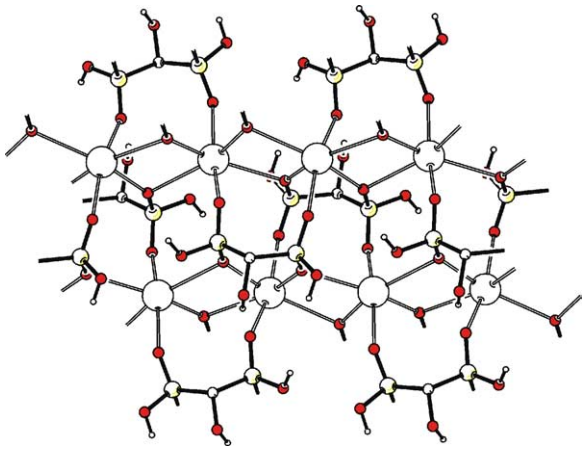

Fig. 20. A view of helical chains in **2**-**41**.

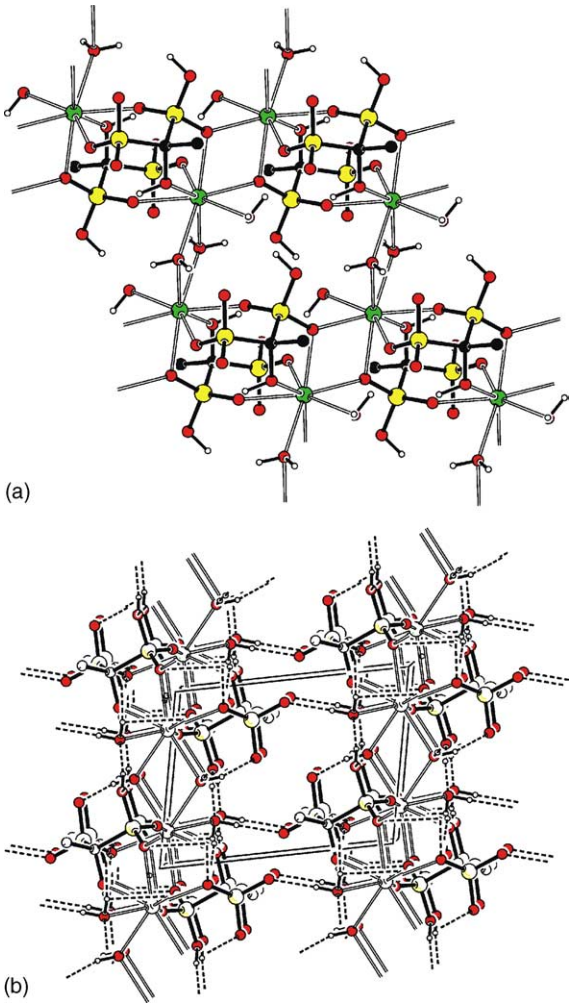

Fig. 21. The intralayer (a) and interlayer (b) connections in **2**-**42**.

9.73 Å between the layers. However, the coordination mode of Ca^{2+} in the **3**-**1** [115] complex is completely different. The hydrogen bonds in this compound seem to play a decisive role for the organization of the anionic network. The inversion related acid moieties are arranged via the hydrogen-bonded $R_2^2(8)$ motif in order to form zig-zag ribbons. The calcium ion, bidentately bonded to the ligands, is arranged from both sides of the ribbon, efficiently preventing direct interactions between the neighboring ribbons. Five water molecules fill in there and serve both as donating sites for the calcium ion and as hydrogen-bond donors and acceptor sites to the acid anions joining the ribbons in 3D. The Ca^{2+} in **3**-**1** is seven-coordinated with geometry of a monocapped trigonal prism.

4. Aminomethane-1,1-diphosphonic acids

4.1. Molecular organization in solid state and solution

A careful structural analysis made for a series of aminomethane-1,1-diphosphonic acids reveals the strong

inclination of these compounds to form 2D hydrogen-bonded monolayers packed in 3D using van der Waals forces and/or weak hydrogen-bond interactions. Similar to **1-3**, the strongest O–H···O hydrogen bonds direct the basic molecular arrangements. However, the steric congestion around the α-carbon atom disallows the formation of 3D hydrogen-bonded networks. Only one-dimensional hydrogen-bonded arrays are displayed in the compounds **6** and **9**. The protonated nitrogen atom, involved in intramolecular hydrogen bonding usually serves to stabilize the one-dimensional arrangement but it can also be used for extension in the second dimension [49,50].

The recognition preferences of the aminomethane-1,1-diphosphonic acids depend upon the peculiarities of the amino moieties. Phosphonate–phosphonate (PO_3H^-–PO_3H^-) and phosphonic–phosphonic (PO_3H_2–PO_3H_2) hydrogen bonds are used in the 1D polymeric extension of **5** (Fig. 22a). Phosphonate–phosphonate and phosphonic–phosphonate interactions form alternating $R_2^2(8)$ and $R_2^2(12)$ dimeric units in **6** (Fig. 22b), while only the alike phosphonate–phosphonate and phosphonic–phosphonic sites are involved in the hydrogen bonds in **7**–**11**. Similar to **6**, all compounds **7**–**11** demonstrate preferences for dimer units with the common $R_2^2(8)$ motif formed by phosphonate–phosphonate interaction. The main factor differentiating the compounds **7**–**11** is the distribution of the non-covalent bonds, which significantly depends upon the topology of substituent on the piperidyl ring. The molecular organization inside the layers as well as the inter-layer relationships in **10**–**11** are different from those in **7**-**8**. On the other hand, the topology of the substituent in **9** does not allow a close approach between the ribbons, and they are linked together exclusively via the water molecules incorporated in the crystal lattice [50].

The *N*-2-pyridylaminomethane-1,1-diphosphonic acids are generally more rigid as compared to **5**-**11** and can adopt two different *Z* or *E* conformations, issued from the partially double bond character of the $C_{(pyridyl)}$–N bond (with a mean value 1.35 Å). The particular packing arrangements of the compounds are strongly dependent upon changes on the pyridyl ring and especially upon the position of the substituent. The exocyclic NH proton in the 3-pyridyl substituted compounds assumes an *E* orientation with respect to the pyridine nitrogen, while the reversed *Z* orientation is adopted by compounds with a substituent at the 5- or 6- position [40,49,51,52]. This phenomenon significantly accounts for the recognition preferences of the molecules. Only phosphonic–phosphonate hydrogen bonding is used for the two-dimensional organization in **12**. The screw related molecules are extended into helical chains, which are further associated into puckered layer [49]. Quite different arrangement occurs in **14**, which crystallizes with a non-centrosymmetric space group and two independent molecules A and B in the asymmetric unit cell. This feature seems to be common for derivatives of *N*-2-pyridylaminomethane-1,1-diphosphonic acid with a

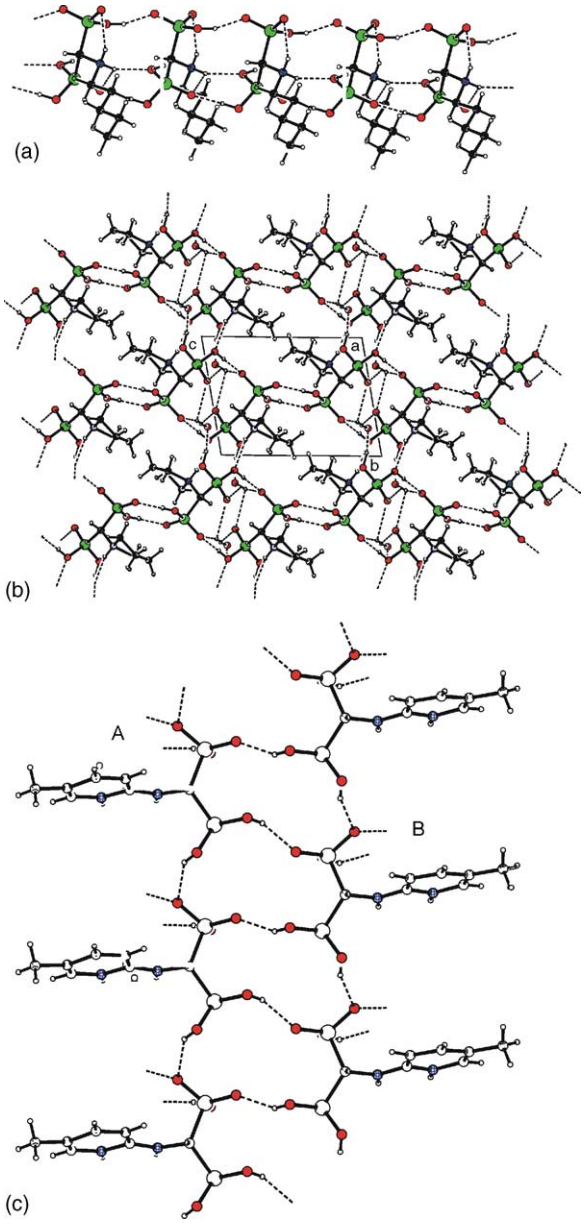

Fig. 22. The molecular ribbon in **5** (a), the hydrogen-bonded monolayer in **6** (b); the A and B chains in **14** (c). Reproduced from Ref. [49] with permission of the copyright holders.

substituent at 5-position on the pirydyl ring [49,52]. Both phosphonic–phosphonate and phosphonate–phosphonate interactions are used for the monolayer formation in **14**. The shortest phosphonic–phosphonate interactions join each A molecule with two B molecules and each B molecule with two A molecules forming trimers, which are further extended into ribbons via weaker phosphonic–phosphonate interactions (Fig. 22c).

Considering the process of crystal disintegration upon dissolution as an opposite to that of a crystal formation we may be able to anticipate the most abundant aggregation forms. The stepwise disruption of the network leads to smaller molecular assemblies, stable under certain con-

ditions in solution. It is apparent that the non-directional packing forces, the weakest intra- and/or intermolecular and the water hydrogen bonds should release first. However, due to the different acidities of the phosphonic–phosphonate groups, the strong intermolecular O–H···O hydrogen bonds established between them break stepwise and this process is essentially dependent on pH. Because of the strong acidity of the PO_3H_2 group the phosphonic–phosphonic or phosphonic–phosphonate hydrogen bonds disconnect first, while some of the phosphonate–phosphonate hydrogen bonds still pertain in solution even under slightly basic conditions. This accounts for the intermolecular metal–ligand interactions leading to formation of multinuclear protonated complexes, whose existence is proved by both NMR and potentiometric methods [45,116].

4.2. Complex-forming abilities

Only a few papers dealing with the metal binding abilities of aminomethane-1,1-diphosphonic acids are available in the literature [45,46,117–119]. They demonstrate a clear preference towards chelation via the phosphonate functions of the ligand similar as it is in **1**-**3**. Despite the incorporation of the amino functionality, the formation of nitrogen-bonded complexes with most compounds of this class is negligible or less important. The strong basicity of the nitrogen proton only permits their formation in alkaline solutions [45]. Compounds **12**-**14** represent a subclass which coordinate metal ions exclusively via phosphonate oxygens, rationalized by sp^2 hybridization of the exocyclic nitrogen atom. Additionally the pyridyl nitrogen is topologically not favorable for metal ion co-ordination [45,46].

However, the differences in coordination abilities of **4**-**14** versus those of **1**-**3** are controlled mainly by the nitrogen center. For example, the presence of the strongly basic and positively charged nitrogen atom in **5**-**11** decreases the net ligand charge at any state of protonation when compared to **1**-**3**. Due to the higher acidity of the PO_3H^- groups, efficiently chelating $[HL]^{3-}$ ligand forms are already available at lower pH values. In addition, for steric and electronic reasons, the amino substituent located on the α-carbon atom probably efficiently prevents the crystallization process of the complexes. To the best of our knowledge there are no single crystal data in the literature concerning a metal complex of aminomethane-1,1-diphosphonic acid. On the other hand, this class of acids tends to form protonated, soluble multinuclear complexes, which is especially notable in the intermediate pH range, at higher concentrations and 1:1 metal-to-ligand molar ratio. This tendency, strongly dependent upon the ligand capacity for aggregate formations in solution, is particularly well expressed for zinc(II). This can be explained with the borderline hardness of the zinc(II) ion and the d^{10} configuration allowing for easy subordination to the steric requirements of the ligand. The pronounced formation of multinuclear complexes in solution is observed as an exceptional broadening of the resonances in the ^{31}P NMR spectra, not detected when the mononuclear complexes are the predominant forms [45].

Combined potentiometric calculations and NMR titration studies showed that $[Zn_4L_3H_3]$ is the major species in the equimolar Zn^{II}-**5** system at a ligand concentration of 1×10^{-2} mol dm^{-3}. The $[Zn_3L_2H_2]$ is formed in Zn^{II}-**6** under similar conditions. Very recent studies demonstrate that compounds **7**-**11** are also capable of forming multinuclear complexes with zinc(II) [116]. If the complex formation process is considered as a gradual replacement of the phosphonic–phosphonate protons by the metal ion, starting at the most easily deprotonating oxygen sites, one can anticipate the formation of $[Zn_4L_3H_3]$ to be based on the ribbon aggregations of **5** that still exist at moderate pH. Analogously the $[Zn_3L_2H_2]$ can be considered as based on different dimeric formations of **6** available in the solution of moderate pH (see Fig. 22 and Scheme 8).

Since the ligand deprotonation in **12** leads to complete destruction of the 2D hydrogen–bonded network, exclusively formed by phosphonic–phosphonate hydrogen bonds, metal ion coordination leads to formation of mononuclear complexes. This was proven by both potentiometry and spectroscopic methods in zinc(II) and copper(II) solutions of **12** and **13** [45,46]. In contrast, the compound **14** displays a pronounced tendency for formation of an oligomeric complex,

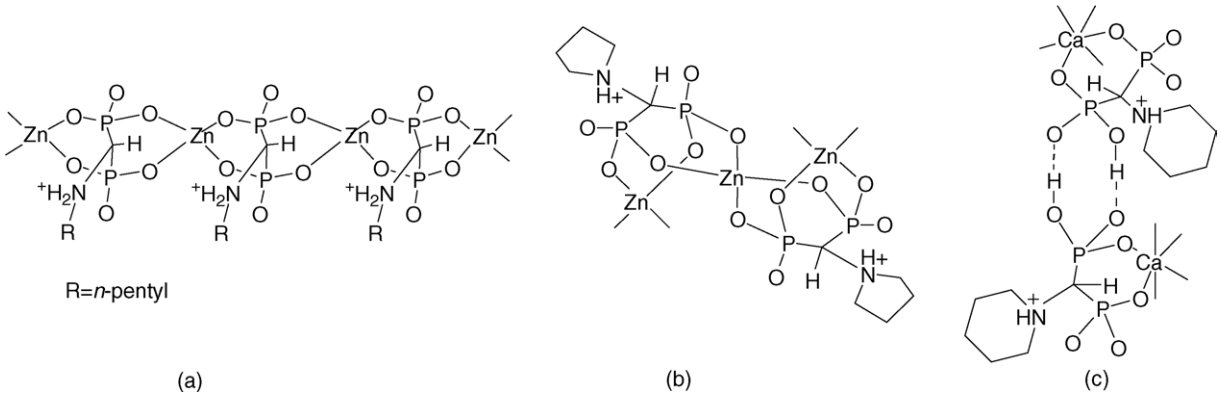

Scheme 8. Tentative solution structures of the $[Zn_4L_3H_3]$ complex of **5** (a), $[Zn_3L_2H_2]$ complex of **6** (b) and $[Ca_2(LH_2)_2]$ complex of **7** [45,116]. The charges are omitted.

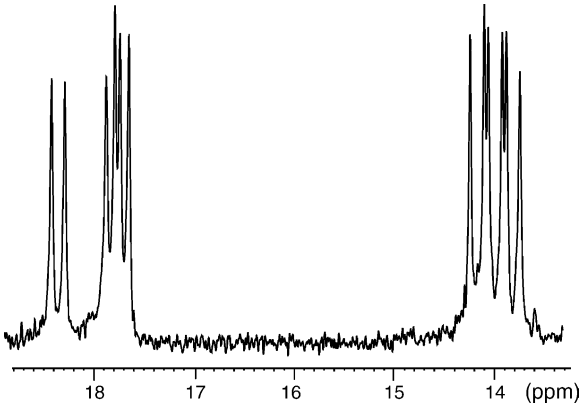

Fig. 23. ^{31}P NMR spectrum for the Zn^{II}-**14** at pH 5.54; $c_M = c_L = 1 \times 10^{-1}$ mol dm^{-3}.

which is reflected in the multiple resonance signals detected in the ^{31}P NMR spectra of the equimolar Zn^{II}-**13** solution at pH ~7–10 (Fig. 23). Similar NMR spectra are observed also in Zn^{II}-**15** and Zn^{II}-**16** [48], which is unique for the zinc(II) systems.

Generally, Mg^{2+} displays less tendency for multinuclear complex formation. Nonetheless, a $[Mg_3L_2H_2]$ species analogous to $[Zn_4L_3H_3]$ (Scheme 8a) is found in the Mg-**5** system. On the other hand, Ca^{2+}, as a bigger and more flexible ion compared to Mg^{2+} tends to form aggregate polymeric complexes, that precipitate. Since bisphosphonate drugs encounter the calcium ions on the bone mineral surface and in solution, one reason for the bisphosphonate divergences in their bone affinities is the difference in the solubility of the calcium complexes [117]. Heterocyclic amines attached as side chains to the α-carbon atom improve the solubility of these calcium complexes. Soluble, mononuclear complexes are formed over the whole pH range in the calcium(II) system with **6** [45], while the $[Ca_2(LH_2)_2]$ complex (Scheme 8) is the major species over the pH range 4–7 in calcium(II) systems with **7**–**11** [116].

Compound **4** and its *N*,*N*-dimethyl analogue form highly stable complexes (log β_{ML} values in the range 30–24.8) with In^{3+}, Fe^{3+}, Ga^{3+} and UO_2^{2+} ions [118,119].

In view of these complexation features, aminomethane-1,1-diphosphonic acids appear to be good candidates for imaging application or as sequestering agents.

5. Iminodimethylenediphosphonic acids

5.1. Molecular organization in the solid state

Introduction of the $-CH_2-NH-CH_2-$ spacer between the phosphonic groups significantly changes the hydrogen-bond potential in favor of the intermolecular over the intramolecular interactions. Only intermolecular N–H···O hydrogen bonds are present in all four crystal structures **15–18** known to date [48,61,62] (Scheme 9). The lower basicity of the nitrogen proton observed in iminodimethylenediphosphonic acids, versus that in aminomethane-1,1-diphosphonic acid and its derivatives can be attributed to the engagement of the nitrogen proton in an intermolecular interaction. On the other hand, the supramolecular networks of **15–18** substantially depend upon the topochemical nature of the substituent attached to the nitrogen atom.

In **15** the dimers (a) (Scheme 9) are extended into ribbons using the $R_4^2(12)$ motif, generated by phosphonic–phosphonate interactions. Phosphonate–phosphonic hydrogen bonds join the ribbons via a $R_2^2(16)$ in order to form formal undulate molecular monolayers. The neighboring inversion related monolayers are interconnected via another N–H···O hydrogen bond donated from the second proton on the nitrogen atom. However, the replacement of one of the nitrogen protons for the larger methyl group in **16** enforces an inclined interpenetration of the formal monolayers issued from 2D extension of the dimers (b). Small $R_4^4(16)$ and the big $R_6^4(32)$ tetrameric motifs are generated in the monolayers, formed from the 2D extension of the dimers. Molecules of **18** use their full hydrogen-bond donor and acceptor capacity in monolayer formation. The dimers (d) are extended into molecular ribbons via a $R_2^2(8)$ motif formed by the phosphonate–phosphonic hydrogen bonds. The phosphonic–phosphonate interactions join the ribbons via $R_4^2(12)$ into a layer. Additional big voids with $R_4^4(24)$ are

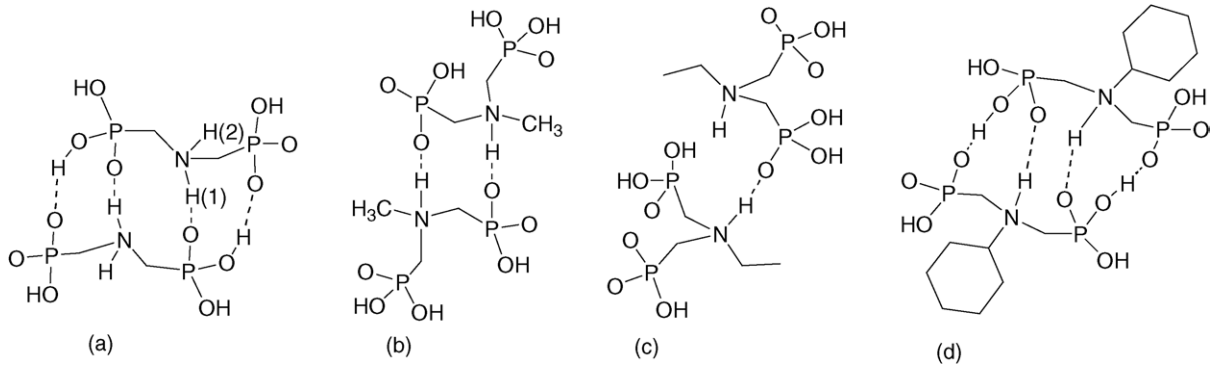

Scheme 9. Intermolecular N–H···O hydrogen bonding. The centrosymmetric dimer is a recurrent motif in **15–18** (except for **17**).

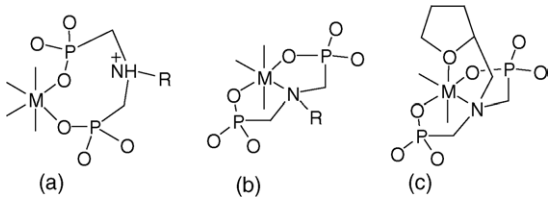

Scheme 10. Di-, tri- and tetradentate coordination modes expected in solutions of iminodimethylenediphosphonic acids with divalent metal ions.

generated between the ribbons of the layer. The cyclohexyl rings, protruding into the voids, are arranged in the exterior between the monolayers. Therefore, the 3D structure of **18** comprises well-defined hydrophilic and hydrophobic regions.

However, a completely different molecular organization is enforced in **17**. The dimer formation is prevented by the ethyl substituent. Instead, the molecules are extended into 1D chains via the shortest O–H···O hydrogen bond and two more O–H···O are joining the chains into molecular ribbons running along the [0 0 1] crystallographic direction. The N–H···O hydrogen bonds interconnect the ribbons in a 3D network, generating channels closed between each four neighboring ribbons, where the ethyl groups are arrayed.

5.2. Complex-forming abilities in solution and solid state

Similar to **1** and **2** the iminodimethylenediphosphonic acids prefer an equimolar metal-to-ligand stoichiometry in solution. However, due to the lower basicity of the imino nitrogen, tridentate species are more easily formed. The extent of their formation as well as the pH region in which they appear depend primarily on the affinity of the particular metal ion towards the nitrogen atom. NMR studies revealed that the soft Pt^{2+} ion coordinates the nitrogen atom of **15** just at pH ∼1 [120]. On the contrary, the hard Mg^{2+} and Ca^{2+} ions are found to predominantly form $[MHL]^{-}$ species with 'pure' phosphonate coordination only [48,121]. Similar (O,O) bonded complexes are found in the systems of Mn^{2+}, Co^{2+} and Ni^{2+} [122]. The attachment of a sterically accessible extra oxygen atom to the imino nitrogen (compound **23**) results in tetradentate coordination with the (O,O,O,N) binding mode (Scheme 10), even for Ca^{2+} [48].

Analogous studies with zinc(II) revealed that zinc coordinates most compounds of this series in a similar way. The resultant $[ZnL]^{-}$ tridentate complex (b) (Scheme 10) predominates in the pH range ∼7–11.5. Quite surprisingly, compounds **15** and **16** behave differently. In particular, in the pH range ∼7–10, the NMR spectra of equimolar solutions demonstrated a non-equivalence of the phosphorus atoms and of the methylene protons, which suggested a significant rigidity of the methylenephosphonate arms involved in the metal co-ordination. The lack of such phenomenon in analogous systems with Ca^{2+} and Mg^{2+} made us to speculate in an earlier paper [48], that the Zn–N binding can be considered as a key factor required for this complex formation. Therefore, we presumed that the spectra correspond to the soluble oligomeric species of a layer-like structure, in which one phosphonate group takes part in (N,O) chelation and bridging, whereas the other binds Zn(II) in a monodentate way. Such a propensity of **15** and **16** was not mentioned in the earlier Sawada studies carried out at a ligand concentration of 5×10^{-4} mol dm^{3-} [121].

The effort to prepare and structurally characterize crystalline metal complexes of iminomethylenediphosphonic acids resulted in several products representing versatile types of structures, variable modes of phosphonate coordination (Table 4; Scheme 11) and different coordination networks. Notably, the majority of structural studies focused on metal complexes of **15** [123–127] and **16** [128–130]. All have a protonated nitrogen atom in their structure, which stands in contrast with the first structurally characterized compound of this series, namely **17-1** [131].

A variety of coordination structures, starting from polymeric chains, and layers to 3D frameworks, are found in metal complexes of iminomethylenediphosphonic acids depending on the reaction conditions and the preferences of the metal ion. The majority of the complexes is obtained under hydrothermal conditions. Their common feature is that the ligand serves as a bridge between the neighboring metal centers. Eight-membered chelate rings are additionally found in crystals **15-4**, **16-2**, **16-3**, **16-4** and **19-1**. All observed coordination units and extending motifs are collected in Scheme 12 and Table 4.

Compounds **15-1**, **15-2** [123,124] are isostructural and display 2D coordination monolayers with large voids of R4,8(32), closed between four metal centers. The C–N–C spacers of two opposite ligands are arranged inside the voids. The monolayers are arranged in stacks with the voids exactly one over the other. A rich hydrogen-bonded network is formed both inside the layers and between them.

Porous 3D coordination frameworks are formed in **15-3** [125] and **15-4** [123,126]. There are two crystallographically distinct tetrahedral centers Co(1) and Co(2) in **15-3** forming two independent coordination networks. Four Co(2) ions are bridged by four ligands in order to form a corrugated 2D network with non-centrosymmetric R4,8(32) rectangular windows. The Co(1) ions generate interlocked rings R4,8(24) and R2,4(16) in order to form 3D coordination frameworks (Fig. 24). The bridging of the four Co(1) centers in the bigger ring takes place via a pair of whole ligands and the phosphonate groups of the other pair of ligands. The two frameworks Co(1) and Co(2) are interpenetrated with two Co(1).

The crystal structure of **15-4** is generated by two symmetry distinct metal centers Cu(1) and Cu(2), each of which forms an independent framework. Cu(2) is octahedral by binding four ligands, two of which are chelated, and forms a 2D coordination net with R4,8(16) windows. Two tetrahedral Cu(1) ions fill in the windows (Fig. 25a), coordinating three ligands from the monolayer and one ligand from the next one, thus linking the monolayers into a 3D coordination

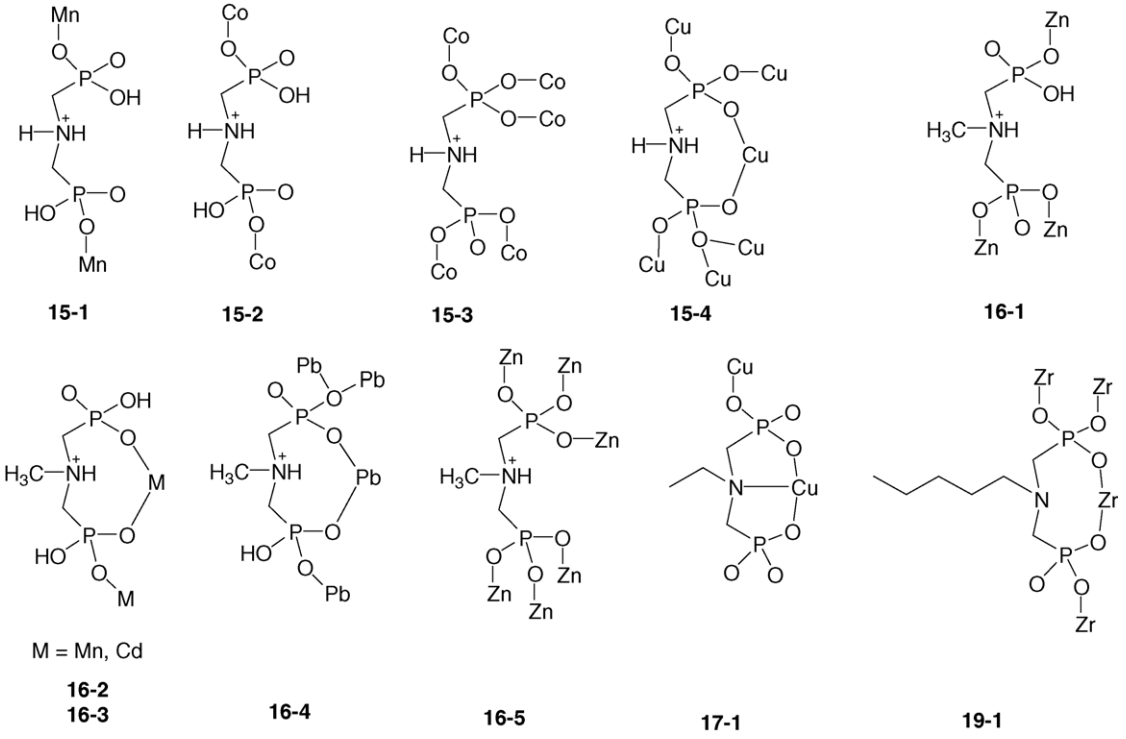

Scheme 11. Coordination modes of **15**–**17** and **19** in complexes with divalent metal ions.

network (Fig. 25b). The corrugated molecular skeletons are arranged in the channels generated along the [0 1 0] direction. Cabeza et al. reported the same compound, obtained by a C–N cleavage reaction after refluxing copper chloride and nitrilotris(methylenephosphonic) acid in water solution at pH ∼2 for 9 days [127].

The zinc ions in **16-1** [128] replace one of the hydrogen atoms of each of the phosphonate groups of the acid, but do not significantly disturb its 2D organization. The molecular dimers (b) (Scheme 9) are preserved as well as the monolayer formation. However, the ring formations in the coordination monolayers are smaller versus those observed for the

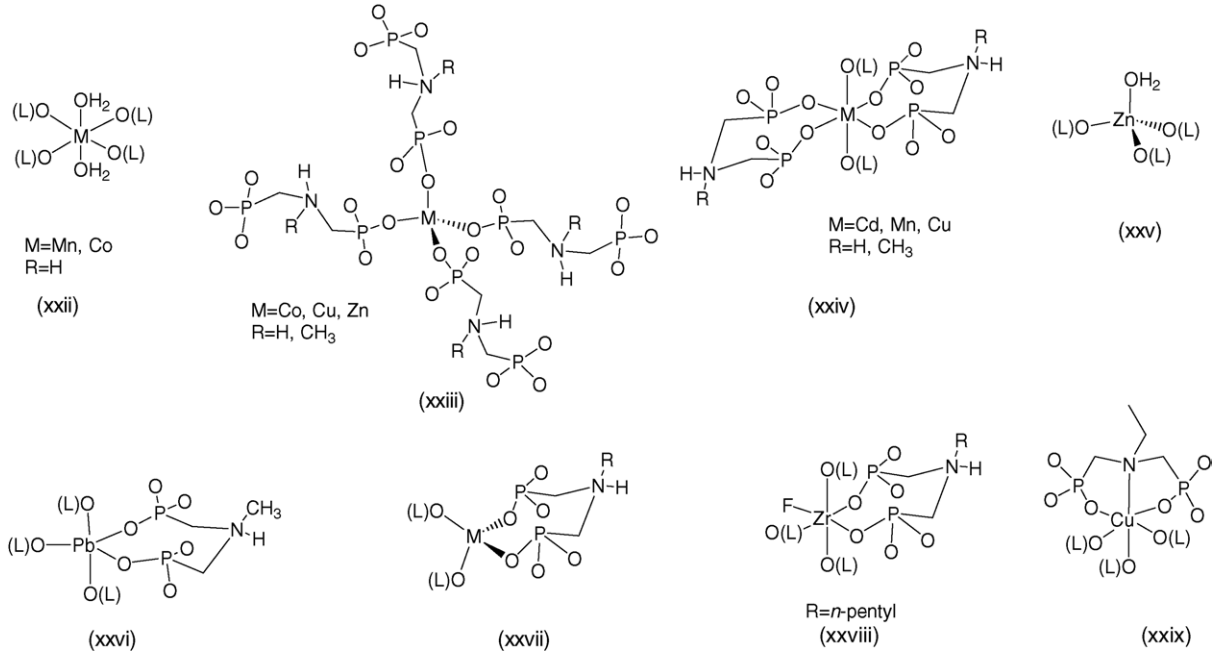

Scheme 12. The coordination units in metal complexes of **15**–**17** and **19**. Hydrogen atoms on the phosphonate groups are not included, if any.

Table 4
The coordination units and the superstructural motifs in the complexes of iminodimethylenediphosphonic acids

No.	Compound formula	Ref. code	Space group	Coordination unit			Ref.
15-1	$[Mn(H_2O)_2(H_2L)_2]$		$P2_1/n$	(xxii)	Hydrogen-bonded monolayers with R4,8(32) voids		[123]
15-2	$[Co(H_2O)_2(H_2L)_2]$	XOGBAW	$P2_1/n$	(xxii)			[124]
15-3	$[Co_3(HL)_2]$	GUZXUU	$P2_12_12_1$	Co(1) (xxiii) Co(2) (xxiii)	2D with R4,8(24) and R2,4(16) windows 2D with R4,8(32) window	3D structure	[125]
15-4	$[Cu_3(HL)_2]$		$Pbca$	Cu(1) (xxiii) Cu(2) (xxiv)	Links the monolayers 2D with R4,8(16)	3D structure	[123,126]
16-1	$[Zn\ H_2O(H_2L)]$	MUNJEK	$P\bar{1}$	(xxv)	Hydrogen-bonded 1D coordination ribbons		[128]
16-2	$[Cd(H_3L)_2]\cdot 2H_2O$	MUNJO	$P\bar{1}$	(xxiv)	Hydrogen-bonded square grid monolayers with R4,8(16) windows		[128]
16-3	$[Mn(H_3L)_2]\cdot 2H_2O$	XIZCAK	$P\bar{1}$	(xxiv)	Hydrogen-bonded square grid monolayers with R4,8(16) windows		[129]
16-4	$[Pb(H_2L)]$	WULYOR	$P2_12_12_1$	Pb(1) (xxvi) Pb(2) (xxvi)	Square grid with R4,8(16) window Square grid with R4,8(16) window	Hydrogen-bonded bilayers	[130]
16-5	$[Zn_3(HL)_2]$	XIZCEO	$P2_1/n$	Zn(1) (xxiii) Zn(2) (xxvii) Zn(3) (xxiii)	1D ribbons, intralayer Joins monolayers in 3D 2D with R4,8(32) voids	3D structure	[129]
19-1	[ZrF(HL)]	TUSVAE01	$P2_1/c$	(xxviii)	Monolayers joined via van der Waals interactions		[132]
17-1	$Cs_2[CuL]\cdot 6H_2O$	JOKWAH	$C2$	(xxix)	1D coordination polymers organized in 3D via counter ions and hydrogen bonding to water		[131]

acid. The tetrahedral zinc ions fasten the hydrogen-bonded dimers (b) and extend them into coordination ribbons along the [0 1 0] direction. The coordination ribbons are further arranged in monolayers via phosphonate–phosphonate interactions, generating smaller hydrogen-bonded motifs $R_2^2(16)$ than those in the pure acid (Fig. 26). The coordinated water molecule serves as hydrogen-bond donor in order to join neighboring parallel monolayers, completing the 3D structure.

The compounds **16-2** [128] and **16-3** [129] are isostructural. Square-grid monolayers with R4,8(16) windows are formed from the interplay of two distinct octahedral metal centers. The crystal water molecules occupy the interlayer region and hydrogen-bond the monolayers. The monolayers are organized in stacks with the windows one above the other in order to form channels where the molecular skeletons are arranged.

In **16-4** both symmetry independent lead ions are five-coordinate with one shorter coordination bond [130]. Each of Pb(1) and Pb(2) forms square grid coordination sheets (Fig. 27) with R4,8(16) windows. The chelated ligand of

Fig. 24. The monolayers with R4,8(32) windows (a) and R2,4(16), R4,8(24) windows (b) formed by Co(2) and Co(1), respectively, in **15-3**.

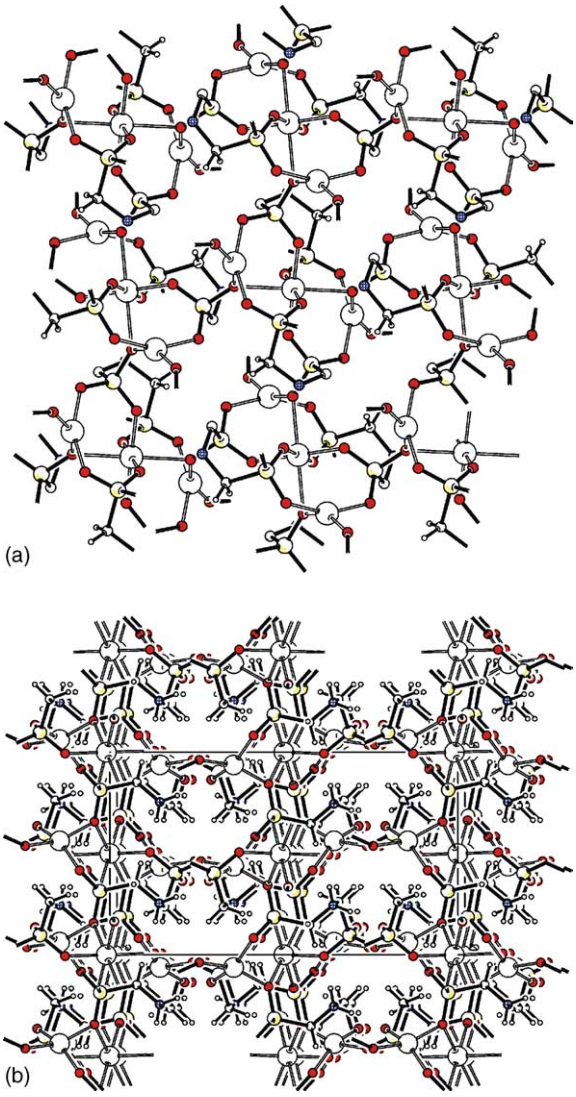

Fig. 25. The Cu(2) monolayer with R4,8(16) windows, two Cu(1) fall into each window (a); a side view of three monolayers bonded in 3D via Cu(1) (b) in **15-4**.

Pb(1) coordination sheet donates the shortest bond towards the Pb(2) ion and vice versa in order to connect the screw related sheets forming a thick bilayer. The skeleton of the chelated ligands protrudes into the window and is arranged in the interior of the bilayer. Neighboring bilayers are connected via two different phosphonate–phosphonate hydrogen bonds. The screw relation between the layers prevents the channel formation in this structure.

The replacement of the coordinated water in **16-1** with an acid ligand gives **16-5** [129]. The tetrahedral geometry of metal ions in **16-5** is retained, however, there are three symmetrically distinct metal centers each forming different coordination species. Four Zn(3) ions monodentately bridged by four ligands form a folded 2D network with R4,8(32) voids, where Zn(1) is residing. Zn(1) displays 1D ribbons extended into 2D via N–H···O. Zn(2) is arranged in the interlayer region and joins the neighboring monolayers via

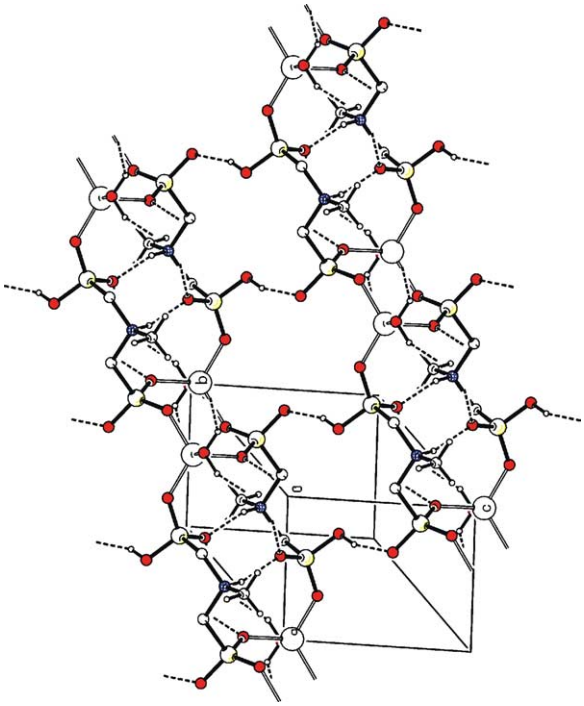

Fig. 26. A view of the polymeric chains in **16-1** hydrogen bonded in order to form monolayer.

alternating centrosymmetric R2,4(16) and R4,8(16) motifs generating channels (Fig. 28).

The interweavement of zirconium helical chains in **19-1** [132] generates coordination ribbons along the *b*-axis, coordinatively extended via translation relation in order to form thick molecular (*bc*) monolayers. The coordinated fluorine ions are sitting on the outer surfaces of the monolayer. The *n*-pentyl side chains, organized outward the monolayer, are interdigitated in order to join the monolayers via van der Waals interactions (Fig. 29), generating hydrophobic regions.

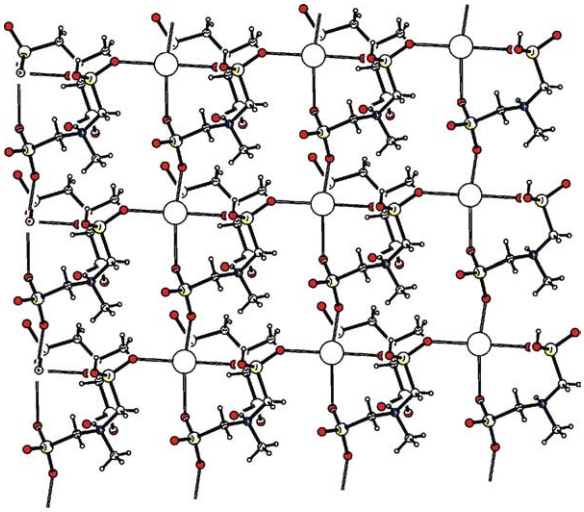

Fig. 27. A view of the 2D network in **16-4**.

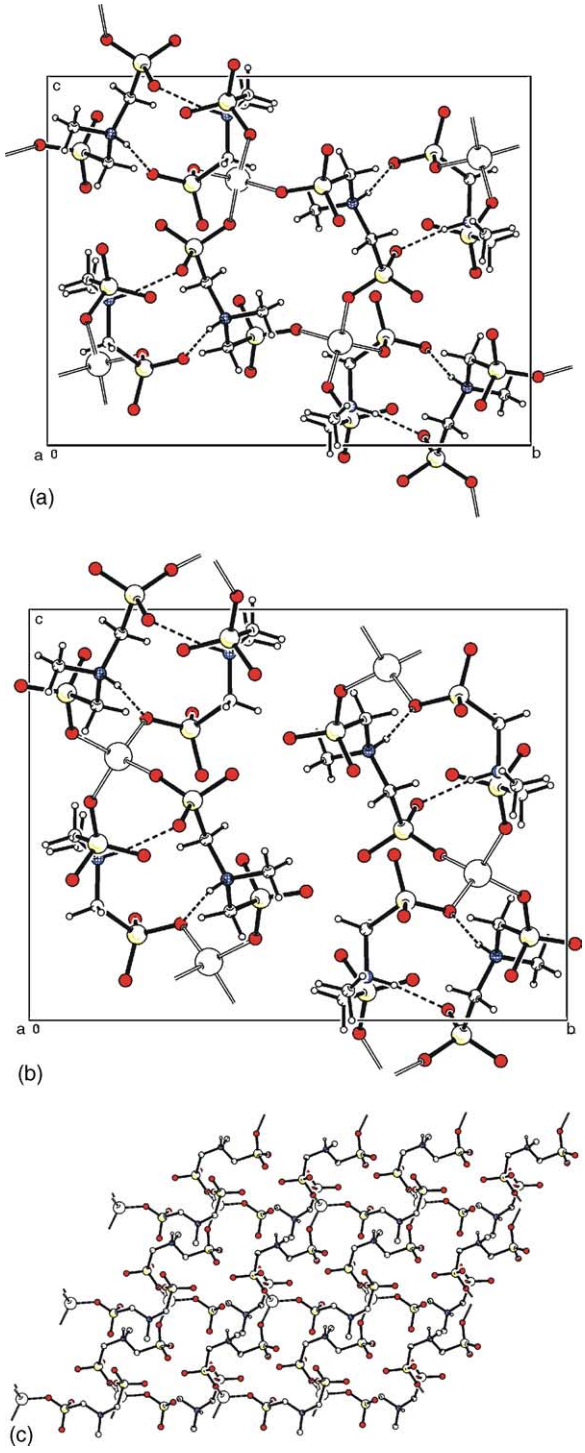

Fig. 28. The dimer of Zn(2) (a); the 1D coordination chain of Zn(1) (b); corrugated 2D framework of Zn(3) (c) in **16-5**.

The only example of tridentate metal coordination is observed in **17-1** [131], with a nitrogen coordinated to the copper ion. The zig-zag Cu coordination polymers along [0 1 0] are organized in monolayers (1 0 0) via the counter cesium ions. The tridentately bonded ligands are arranged from both sides of the monolayers. The second cesium ion and the crystal water molecules reside in the interlayer region

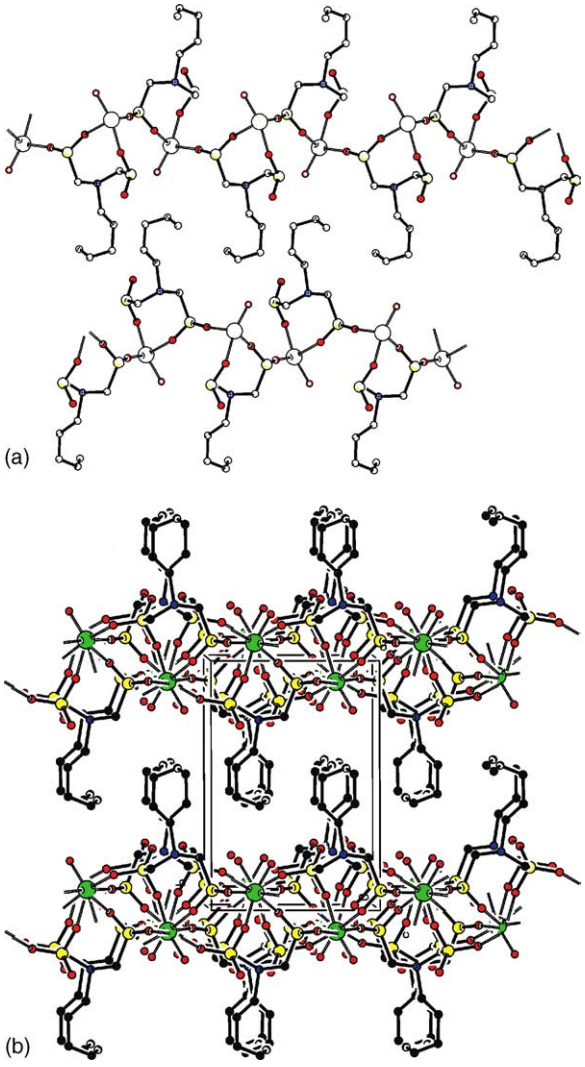

Fig. 29. A view of two opposite running helices belonging to two different layers (a); a side view of two neighboring monolayers and the relationships in between (b) in **19-1**.

and join the monolayers via a rich hydrogen-bond network and Cs–O bonds.

The flexibility of methylene phosphonate arms in **16-1** and **16-2**, regardless of the experimental conditions (conventional or hydrothermal), fulfills the geometrical requirements of the tetrahedral zinc(II) ion without breaking the hydrogen-bonded dimer (b) (Scheme 9). The complex **16-1**, especially, obtained under conventional conditions [128] may be considered as a precursor of the oligomeric complex detected in the Zn(II)-**16** system in the pH range ∼7–10.5 [48]. Most probably the complex is formed upon the gradual release of the protons from the PO_3H^- groups, with resultant breaking of the monolayers (Fig. 26) but preserving the chains. The additional co-ordination stabilization of the hydrogen-bonded dimer, prevents the nitrogen from losing its proton, and the dimer formations are retained even in basic solution (pH ∼10.5). Analogously, the formation of the zinc(II) oligomeric complex with **14** can be considered as based on

the 1D chains (see Fig. 22c). The NMR spectrum (Fig. 23) suggests that the metal ions in this case are presumably coordinated to at least three different ligands using PO_3H^- and PO_3^{2-} groups, each in different chemical environments.

6. Conclusion

As demonstrated from the structural analysis of methane-1,1-diphosphonic (**1**) and 1-hydroxyethane-1,1-diphosphonic acid (**2**), different aggregate formation can arise from the various phosphonate–phosphonate interactions in solutions. However, the dimer formation characterized with the $R_2^2(8)$ motif is the most preferable equilibrium form in solution and therefore is considered to be the basic crystal building block. Indeed, only mono- and dinuclear complexes are observed in solution studies. Nonetheless some tetrameric aggregate formations with $R_3^3(16)$ or $R_4^2(16)$ motifs may also exist in solution.

The bidentate and bis-bidentate binding ability is a discernable feature of **1** and **2**. A tridentate chelation is also found in the complexes of **2**. The analysis made for more than 60 complexes of **1** and **2** reveals an amazing structural diversity with more than 40 different coordination units and linking motifs. It is remarkable that the complexes of **1** can display a whole spectrum of extended frameworks starting from 1D, through 2D and finally 3D. The hydroxylic group in **2** can also participate in bidentate and tridentate co-ordination. However, it never appears in a deprotonated form. The vast majority of complexes of **2** form 1D polymeric chains or appear as isolated monomers and dimers. Only five compounds display 2D species and no representatives with 3D coordination framework are found. The main reason for that may be the steric impediment imposed by the methyl group. However, the lack of deprotonation in the hydroxylic group is not to neglect in systems with hydrogen-bond acceptors and the hydroxylic proton may play role for the supramolecular preferences in these compounds. On the other hand, the replacement of a C_α hydrogen atom for the substituted amino group introduces severe steric and electronic changes and drastically impedes the ligand adaptability to the close packing requirements of the crystal. No any single complex is found in a crystal form, although mono and multinuclear complexes are proved to be formed in solution of aminomethane-1,1-diphosphonic acids.

As far as the iminodimethylenediphosphonic acids are concerned, the C–N–C spacer is responsible for the significantly changed coordination ability of the ligands. The more acidic nitrogen proton enables the nitrogen to co-ordinate as well, which is documented by solution studies. Even so, only one crystal with a tridentate coordination is reported. Another characteristic feature of this class of compound is that the bridging of the metal centers takes place via both end-positioned phosphonate groups. Despite the fact that the eight-membered chelate ring is considered as being less stable, it is found in half of these complexes.

It is obvious that a careful analysis of the topology of a given class of compounds is unavoidable in the attempt to establish useful relationships between structure and properties. The structural aspects presented in this review might be important for elaborating new concepts in the crystal engineering and supramolecular chemistry of bisphosphonates. Finally, the results of the comparative studies made above can be employed to design a number of novel prototypical network structures based upon selected building blocks.

Acknowledgement

The financial support from the Polish State Committee for Scientific Research (Project PBZ-KBN-060/T09/2001/14) is thankfully acknowledged.

References

[1] L.J.M.J. Blomen, in: O.L.M. Bijvoet, H.A. Fleish, R.E. Canfield, R.G.G. Russel (Eds.), Bisphosphonates on Bones, Elsevier, Amsterdam, 1995, p. 111.
[2] H. Fleisch, R.G.G. Russel, F. Straumann, Nature 212 (1966) 901.
[3] G.A. Rodan, R. Balena, Ann. Med. 25 (1993) 373.
[4] R.G.G. Russel, Phosphorus Sulfur Silicon 144–147 (1999) 793.
[5] G.A. Rodan, T.J. Martin, Science 289 (2000) 1508.
[6] L. Widler, K.A. Jaeggi, M. Glatt, K. Müller, R. Bachmann, M. Bisping, A.-R. Born, R. Cortesi, G. Guiglia, H. Jeker, R. Klein, U. Ramseier, J. Schmid, G. Schreiber, Y. Seltenmeyer, J.R. Green, J. Med. Chem. 45 (2002) 3721.
[7] R.G.G. Russel, P.I. Croucher, M.J. Rogers, Osteoporosis 2 (Suppl.) (1999) S66.
[8] M.J. Rogers, J.C. Frith, S.P. Luckman, F.P. Cox, H.L. Benford, J. Mönkkönen, S. Auriola, K.M. Chilton, R.G.G. Russell, Bone 24 (1999) 73s.
[9] R.G.G. Russell, M.J. Rogers, Bone 25 (1999) 97.
[10] E. Van Beek, E. Pieterman, L. Cohen, C. Löwik, S. Papapoulos, Biochem. Biophys. Res. Commun. 255 (1999) 491.
[11] E. Van Beek, E. Pieterman, L. Cohen, C. Löwik, S. Papapoulos, Biochem. Biophys. Res. Commun. 264 (1999) 108.
[12] K.R. Keller, S.J. Fliesler, Biochem. Biophys. Res. Commun. 266 (1999) 560.
[13] J.E. Dunford, K. Thomson, F.P. Coxon, S.P. Luckman, F.M. Hahn, C.D. Poulter, F.H. Ebetino, M.J. Rogers, J. Pharmacol. Exp. Ther. 296 (2001) 235.
[14] J.D. Bergstrom, R.G. Bostedor, P.J. Masarachia, A.A. Reszka, G. Rodan, Arch. Biochem. Biophys. 373 (2000) 231.
[15] K. Thompson, J.E. Dunford, F. Ebetino, M.J. Rogers, Biochem. Biophys. Res. Commun. 290 (2002) 869.
[16] E.R. Van Beek, C.W.G.M. Löwik, S.E. Papapoulous, Bone 30 (2002) 64.
[17] M.B. Martin, W. Arnold, H.T. Heath III, J.A. Urbina, E. Oldfield, Biochem. Biophys. Res. Commun. 263 (1999) 754.
[18] D.J. Hosfield, Y. Zhang, D.R. Doughan, A. Broun, L.W. Tari, R.V. Swanson, J. Finn, J. Biol. Chem. 279 (2004) 8526.
[19] M.B. Martin, J.S. Grimley, J.C. Lewis, H.T. Heath III, B.N. Bailey, H. Kendrick, V. Yardley, A. Caldera, R. Lira, J.A. Urbina, S.N.J. Moreno, R. Docampo, S.L. Croft, E. Oldfield, J. Med. Chem. 44 (2001) 909.
[20] A. Montalvetti, B.N. Bailey, M.B. Martin, G.W. Severin, E. Oldfield, R. Docampo, J. Biol. Chem. 276 (2001) 33930.

[21] V. Yardley, A.A. Khan, M.B. Martin, T.R. Slifer, F.G. Araujo, S.N.J. Moreno, R. Docampo, S.L. Croft, E. Oldfield, Antimicrob. Agents Chemother. (2002) 929.
[22] L. Garzoni, A. Caldera, M. De Nazareth, L. Meirelles, S.L. De Castro, R. Docampo, G.A. Meints, E. Oldfield, J.A. Urbina, Int. J. Antimicrob. Agents 23 (2004) 273.
[23] L.R. Garzoni, M.C. Waghabi, M.M. Baptista, S.L. De Castro, M. De Nazareth, L. Meirelles, C.C. Britto, R. Docampo, E. Oldfield, J.A. Urbina, Int. J. Antimicrob. Agents 23 (2004) 286.
[24] J.M. Sanders, A.O. Gómez, J. Mao, G.A. Meints, E.M. Van Brussel, A. Burzyńska, P. Kafarski, D. González-Pacanowska, E. Oldfield, J. Med. Chem. 46 (2003) 5171.
[25] A. Montalvetti, A. Fernandez, J.M. Sanders, S. Ghosh, E. Van Brussel, E. Oldfield, R. Docampo, J. Biol. Chem. 278 (2003) 17075.
[26] E. Grossband, D. Atkinson (Eds.), The Herbicide Glyphosate, CRC Press, Boca, Raton, FL, 1989.
[27] P. Kafarski, B. Lejczak, G. Forlani, R. Gancarz, C. Torreilles, J. Grembecka, A. Ryczek, P. Wieczorek, J. Plant. Growth Regul. 16 (1997) 153.
[28] A. Clearfield, in: K.D. Karlin (Ed.), Progress in Inorganic Chemistry, vol. 47, J. Wiley & Sons Inc., New York, 1998, p. 371.
[29] A. Clearfield, Z. Wang, Dalton (2002) 2937.
[30] D.L. Lohse, S.C. Sevov, Angew. Chem. Int. Ed. Engl. 36 (1997) 1619.
[31] T.J. Marks, M.A. Ratner, Angew. Chem. Int. Ed. Engl. 34 (1995) 155.
[32] G.A. Neff, M.R. Helfrich, C.J. Page, Phosphorus Sulfur Silicon Relat. Elem. 144–146 (1999) 53.
[33] G.A. Neff, M.R. Helfrich, M.C. Clifton, C.J. Page, Chem. Mater. 12 (2000) 2363.
[34] F.H. Allen, Acta Crystallogr. Sect. B 58 (2002) 380.
[35] F.H. Allen, W.D.S. Motherwell, Acta Crystallogr. Sect. B 58 (2002) 407.
[36] I.J. Bruno, J.C. Cole, P.R. Edgington, M. Kessler, C.F. Macrae, P. McCabe, J. Pearson, R. Taylor, Acta Crystallogr. Sect. B 58 (2002) 389.
[37] B.F. Abrahams, B.F. Hoskins, R. Robson, J. Am. Chem. Soc. 113 (1991) 3606.
[38] S.R. Batten, R. Robson, Angew. Chem. Int. Ed. Engl. 37 (1998) 1460.
[39] L. Carlucci, G. Ciani, D.M. Prosperio, Coord. Chem. Rev. 246 (2003) 247.
[40] E. Matczak-Jon, Pol. J. Chem. 79 (2005) 445.
[41] S. Bouhsina, P. Buglyó, A. Abi Aad, A. Aboukais, T. Kiss, Inorg. Chim. Acta 357 (2004) 305.
[42] M. Dyba, M. Jeżowska-Bojczuk, E. Kiss, T. Kiss, H. Kozłowski, Y. Leroux, D. El Manouni, J. Chem. Soc., Dalton Trans. (1996) 1119.
[43] E. Gumienna-Kontecka, J. Jezierska, M. Lecouvey, Y. Leroux, H. Kozłowski, J. Inorg. Biochem. 89 (2002) 13.
[44] E. Gumienna-Kontecka, R. Silvagni, R. Lipinski, M. Lecouvey, F.C. Marincola, G. Crisponi, V.M. Nurchi, Y. Leroux, H. Kozłowski, Inorg. Chim. Acta 339 (2002) 111.
[45] E. Matczak-Jon, B. Kurzak, A. Kamecka, P. Kafarski, Polyhedron (2002) 321.
[46] B. Boduszek, M. Dyba, M. Jeżowska-Bojczuk, T. Kiss, H. Kozłowski, J. Chem. Soc., Dalton Trans. (1997) 973.
[47] B. Kurzak, A. Kamecka, K. Kurzak, J. Jezierska, P. Kafarski, Polyhedron 17 (1998) 4403.
[48] E. Matczak-Jon, B. Kurzak, A. Kamecka, W. Sawka-Dobrowolska, P. Kafarski, J. Chem. Soc., Dalton Trans. (1999) 3627.
[49] E. Matczak-Jon, W. Sawka-Dobrowolska, P. Kafarski, V. Videnova-Adrabińska, New J. Chem. 25 (2001) 1447.
[50] E. Matczak-Jon, V. Videnova-Adrabińska, A. Burzyńska, P. Kafarski, T. Lis, Chem. Eur. J. 11 (2005) 2357.
[51] Ch.M. Szabo, M.B. Martin, E. Oldfield, J. Med. Chem. 45 (2002) 2894.
[52] J.M. Sanders, A.O. Gómez, J. Mao, G.A. Meints, E.M. Van Brussel, A. Burzyńska, P. Kafarski, D. González-Pacanowska, E. Oldfield, J. Med. Chem. 46 (2003) 5171.
[53] D. DeLaMatter, J.J. McCullought, C. Calvo, J. Phys. Chem. 77 (1973) 1146.
[54] J.-P. Silvestre, N.Q. Dao, G. Heger, A. Cousson, Phosphorus Sulfur Silicon Relat. Elem. 177 (2002) 277.
[55] V.A. Uchtman, R.A. Gloss, J. Phys. Chem. 76 (1972) 1298.
[56] L.M. Shokol'nikova, S.S. Sotman, E.G. Afonin, Kristallografiya 35 (1990) 1442.
[57] A. Neels, H. Stoeckli-Evans, B. Costistella, H. Jancke, K.D. Knudsen, P. Pattison, Helv. Chim. Acta 82 (1999) 35.
[58] M.P. Jensen, J.V. Beitz, R.D. Rogers, K.L. Nash, Dalton (2000) 3058.
[59] E.M. Van Brussel, W.L. Gossman, S.R. Wilson, E. Oldfield, Acta Cryst. Sect. C 59 (2003) o93.
[60] D. Fernandez, D. Vega, J.A. Ellena, Acta Cryst. Sect. C 59 (2003) o289.
[61] L.M. Shkolnikova, G.V. Polyanchuk, N.M. Dyatlova, T. Ya. Medved, I.B. Goryunova, 2.2 M.I. Kabachnik, Izv. Akad. Nauk SSSR, Ser. Khim. (1985) 1035.
[62] B.I. Makaranets, T.N. Polynova, V.K. Bel'skii, S.A. Il'chev, M.A. Porai-Koshits, Zh. Strukt. Khim. 26 (1985) 131.
[63] M. Etienne, P. Rubini, J. Bessiere, A. Walcarius, C. Grison, P.H. Coutrot, Phosphorus Sulfur Silicon 161 (2000) 75.
[64] L. Alderighi, A. Vacca, F. Cecconi, S. Midollini, E. Chinea, S. Dominiguez, A. Valle, D. Dakternieks, A. Duthie, Inorg. Chim. Acta 285 (1999) 39.
[65] T.A. Matkovskaya, L.S. Nikolayeva, E.A. Mezhonova, T.M. Balashova, A.M. Evseev, N.M. Dyatlova, Russ. J. Inorg. Chem. 34 (1989) 1100.
[66] E.N. Rizkalla, M.T.M. Zaki, M.I. Ismail, Talanta 27 (1980) 715.
[67] H. Wada, Q. Fernado, Anal. Chem. 43 (1971) 751.
[68] V. Deluchat, B. Serpaud, C. Caullet, J.-C. Bollinger, Phosphorus Sulfur Silicon 104 (1995) 81.
[69] V. Deluchat, J.-C. Bollinger, B. Serpaud, C. Caullet, Talanta 44 (1997) 897.
[70] S. Lacour, V. Deluchat, J.-C. Bollinger, B. Serpaud, Environ. Technol. 20 (1999) 249.
[71] R.I. Carrol, R.R. Irani, Inorg. Chem. 6 (1967) 1994.
[72] M.C. Etter, J. McDonald, J. Bernstein, Acta Crystallogr. Sect. B46 (1990) 256.
[73] M.C. Etter, Acc. Chem. Res. 23 (1990) 120.
[74] For the sake of clarity, the alternative notation $R_d^a(n)$ is used throughout this paper for characterizing the hydrogen-bonded ring motifs where *a* means the number of hydrogen-bond acceptors, *d*—number of hydrogen bond donors (proton donors), *n*—number of atoms in the ring.
[75] M. Sundaralingam, Inorg. Chem. 23 (1984) 2412.
[76] Distler, D.L. Lohse, S.C. Sevov, Dalton (1999) 1805.
[77] H.G. Harvey, S.J. Teat, Ch.C. Tang, L.M. Cranswick, M.P. Attfield, Inorg. Chem. 42 (2003) 2428.
[78] C. Nindaus, C. Serre, D. Riou, G. Férey, C.R. Acad. Sci., Ser. M. Chim. 1 (1998) 551.
[79] M. Riou-Cavellec, C. Serre, J. Robino, M. Noguès, J.-M. Grenèche, G. Férey, J. Solid State Chem. 147 (1999) 122.
[80] K. Barthelet, M. Nogues, D. Riou, G. Férey, Chem. Mater. 14 (2002) 4910.
[81] Q. Gao, N. Guillou, M. Nogues, A.K. Cheetham, G. Férey, Chem. Mater. 11 (1999) 2937.
[82] C. Serre, G. Férey, J. Mater. Chem. 12 (2002) 2367.
[83] K. Barthelet, D. Riou, G. Férey, Solid State Sci. 4 (2002) 841.
[84] E. Burkholder, V.O. Golub, Ch.J. O'Connor, J. Zubieta, Inorg. Chim. Acta 340 (2002) 127.
[85] G. Serre, G. Fèrey, Inorg. Chem. 38 (1999) 5370.
[86] K. Barthelet, C. Merlier, C. Serre, M. Riou-Cavellec, D. Riou, G. Férey, J. Mater. Chem. 12 (2002) 1132.

[87] P. Zuohua, J. Xianglin, S. Meicheng, Z. Ruifang, X. Yongzhuang, Chem. J. Chin. Uni. 6 (1985) 69.
[88] K.A. Lyssenko, V.M. Akimov, P.N. Abakunov, Yu. Struchkov, M.A. Ershov, Zh. Neorg. Khim. 42 (1997) 1283.
[89] V.S. Sergienko, G.G. Aleksandrov, E.G. Afonin, Zh. Neorg. Khim. 42 (1997) 1291.
[90] V.S. Sergienko, E.G. Afonin, G.G. Aleksandrov, Zh. Neorg. Khim. 43 (1998) 1002.
[91] V.S. Sergienko, E.G. Afonin, G.G. Aleksandrov, Koord. Khim. 25 (1999) 133.
[92] V.S. Sergienko, G.G. Aleksandrov, E.G. Afonin, Crystallogr. Rep. 45 (2000) 262.
[93] H.-H. Song, Li-Min Zheng, Ch.-H. Lin, S.-L. Wang, X.-Q. Xin, S. Gao, Chem. Mater. 11 (1999) 2382.
[94] V.S. Sergienko, E.G. Afonin, G.G. Alexandrov, Koord. Khim. 24 (1998) 293.
[95] V.S. Sergienko, G.G. Alexandrov, E.G. Afonin, Koord. Khim. 25 (1999) 451.
[96] E.G. Afonin, G.G. Aleksandrov, V.S. Sergienko, Koord. Khim. 25 (1999) 923.
[97] G.G. Alexandrov, V.S. Sergienko, Kristallografiya 44 (1999) 1061.
[98] A. Neuman, A. Safsaf, H. Gillier, Y. Leroux, D. El Manouni, Phosphorus Sulfur Silicon 70 (1992) 273.
[99] G.G. Aleksandrov, E.G. Afonin, V.S. Sergienko, Koord. Khim. 26 (2000) 547.
[100] N. El Messbahi, J.-P. Silvestre, N.Q. Dao, M.-R. Lee, Y. Leroux, A. Neuman, H. Gillier-Pandraud, Phosphorus Sulfur Silicon 164 (2000) 45.
[101] R. Rochdaoui, J.-P. Silvestre, N.Q. Dao, M.-R. Lee, A. Neuman, Acta Crystallogr. Sect. C 48 (1992) 2132.
[102] G.G. Aleksandrov, V.S. Sergienko, E.G. Afonin, Zh. Neorg. Khim. 42 (1997) 1287.
[103] G.G. Aleksandrov, V.S. Sergienko, E.G. Afonin, Zh. Neorg. Khim. 43 (1998) 1811.
[104] V.S. Sergienko, G.G. Aleksandrov, E.G. Afonin, Koord. Khim. 24 (1998) 455.
[105] L.-M. Zheng, H.-H. Song, Ch.-Y. Duan, X.-Q. Xin, Inorg. Chem. 38 (1999) 5061.
[106] H.-H. Song, L.-M. Zheng, Y.-J. Liu, X.-Q. Xin, A.J. Jacobson, S. Decurtins, Dalton (2001) 3274.
[107] H.-H. Song, L.-M. Zheng, G. Zhu, Z. Shi, S. Feng, S. Gao, Z. Hu, X.-Q. Xin, J. Solid State Chem. 164 (2002) 367.
[108] H.-H. Song, L.-M. Zheng, Z. Wang, Ch.-H. Yan, X.-Q. Xin, Inorg. Chem. 40 (2001) 5024.
[109] H.-H. Song, P. Yin, L.-M. Zheng, J.D. Krop, A.J. Jacobson, S. Gao, X.-Q. Xin, Dalton (2002) 2752.
[110] L.-M. Zheng, H.-H. Song, Ch.-H. Lin, S.-L. Wang, Z. Hu, Z. Yu, X.-Q. Xin, Inorg. Chem. 38 (1999) 4618.
[111] H.-H. Song, L.-M. Zheng, G.-S. Zhu, Z. Shi, S.-H. Feng, S. Gao, X.-Q. Xin, Chin. J. Inorg. Chem. 18 (2002) 67.
[112] L.-M. Zheng, S. Gao, H.-H. Song, S. Decurtins, A.J. Jacobson, X.-Q. Xin, Chem. Mater. 14 (2002) 3143.
[113] J.-P. Silvestre, N.El. Messabahi, R. Rochdaoui, N.Q. Dao, M.-R. Lee, A. Neuman, Acta Crystallogr. Sect. C 46 (1990) 986.
[114] V.A. Uchtman, J. Phys. Chem. 76 (1972) 1304.
[115] M. Nardelli, G. Pelizzi, G. Staibano, E. Zucchi, Inorg. Chim. Acta 80 (1983) 259.
[116] E. Matczak-Jon, V. Videnova-Adrabińska, P. Kafarski, B. Kurzak, A. Woźna, Seventh Europ. Biol. Inorg. Chem. Conference 'EUROBIC 7', Garmisch-Partenkirchen, Germany, 2004, p. 239 (Book of Abstracts).
[117] M. Kontturi, E. Vuokila-Laine, S. Peräniemi, T.T. Pakkanen, J.J. Vepsäläinen, M. Ahlgrén, Dalton (2002) 1969.
[118] J.E. Bollinger, D.M. Roundhill, Inorg. Chem. (1993) 2821.
[119] J.E. Bollinger, D.M. Roundhill, Inorg. Chem. (1994) 6421.
[120] T. Appleton, J.R. Hall, I.J. McMahon, Inorg. Chem. 25 (1986) 726.
[121] K. Sawada, T. Kanda, Y. Naganuma, T. Suzuki, J. Chem. Soc., Dalton Trans. (1993) 2557.
[122] B. Kurzak, A. Kamecka, K. Kurzak, J. Jezierska, P. Kafarski, Polyhedron (2000) 2083.
[123] D. Kong, Y. Li, X. Ouyang, A.V. Prosvirin, H. Zhao, J.H. Ross Jr., K.R. Dunbar, A. Clearfield, Chem. Mater. 16 (2004) 3020.
[124] H. Jankovics, M. Daskalakis, C.P. Raptopoulou, A. Terzis, V. Tangoulis, J. Giapintzakis, T. Kiss, A. Salifoglou, Inorg. Chem. 41 (2002) 3366.
[125] A. Turner, P.-A. Jaffrès, E.J. MacLean, D. Villemin, V. McKee, Dalton (2003) 1314.
[126] D. Kong, Y. Li, J.H. Ross Jr., A. Clearfield, Chem. Commun. (2003) 1720.
[127] A. Cabeza, S. Bruque, A. Guagliardi, M.A.G.J. Aranda, J. Solid State Chem. 160 (2001) 278.
[128] J.-G. Mao, Z. Wang, A. Clearfield, Dalton (2002) 4457.
[129] J.-G. Mao, Z. Wang, A. Clearfield, Inorg. Chem. 41 (2002) 2334.
[130] J.-G. Mao, Z. Wang, A. Clearfield, Inorg. Chem. 41 (2002) 6106.
[131] B.I. Makaranets, T.N. Polynova, N.D. Mitrofanova, M.A. Porai-Koshits, J. Struct. Chem. 32 (1991) 116.
[132] U. Costantino, M. Nocchetti, R. Vivani, J. Am. Chem. Soc. 124 (2002) 8428.